The popular democratic republic of Algeria

Ministère de l'Enseignement superieur et de la Recherche Scientifique

Department: Renewable energies

Master 2 Graduation Thesis

Specialty : Solar Heat Conversion

The design, built and experimental test of a solar thermoelectric generator

By :

Oussama Bessedik

Advisor professor:

Dr. Said Noureddine

Defense committee :

- **Mr. M.merzouk**
- **Mr. S.Mihoub**
- **Mr.M.Nehal**

2015 - 2016

Abstract:

Since antiquity, alimentation and heating presented a fundamental need for human, and as he discovered fire and learned to control his life condition started to get better ,but he always wanted more ,so he start to diversify his productions and uses of thermal energy .

One of the uses of thermal energy is the thermoelectric conversion which allows generating electricity from the heat available through thermoelectric conversion devices (Seebeck effect). It appears as one of other alternative method of clean energy production, it is already proven utility such as the production of electrical energy to distant spacecraft. In addition to this power supply aspects thermoelectric materials are used for cooling (Peltier) with many applications in the electronics field.

There are many different thermal sources used in electrical heat such as solar heat, fuel oil, biomass, waste heat from various industries ... etc. But when it comes to work on solar thermoelectric systems, it remains as laboratory scale tests only, because until now we have not had the results that allow us to use the applied scale or industrial. However works are still continuing to improve conditions and optimize results

In this work we make a solar thermoelectric system using a parabolic concentrator to generate the necessary heat to operate the thermo generator. And we study the influence of different parameters (temperature, radiation ...) on the performance of the heat generator.

Résume:

L'alimentation et le chauffage sont des besoins fondamentaux de l'être humain depuis l'antiquité, et depuis qu'il a appris a maîtrisé le feu, ça lui a permis d'améliorer ses conditions de vie et satisfaire à ses exigences temporairement, avant qu'il commence à en vouloir plus, alors ça l'a poussé a chercher à diversifier ses moyens de production d'énergie thermique, puis à diversifier les formes d'énergie.

La conversion thermoélectrique comme d'autres sources alternatives (énergie éolienne, énergie solaire) permet de générer de l'électricité à partir de la chaleur disponible, par le biais de dispositifs de conversions thermoélectriques (effet Seebeck), et apparaît donc comme l'un des procédés alternatifs de production d'énergie propre. Cette dernière a déjà fait ses preuves, notamment comme la production d'énergie électrique pour les sondes spatiales lointaines. Outre cet aspect d'apport d'électricité les matériaux thermoélectriques sont utilisés pour la réfrigération (effet Peltier) avec de nombreuses applications dans le domaine de l'électronique.

Il existe de différentes sources thermiques utilisés dans la thermo électrique tel que la chaleur solaire, le fuel, la biomasse, la chaleur perdue des divers industries …etc. Sauf que quand il s'agit des travaux portant sur les systèmes thermoélectriques solaire sa reste toujours des essais et à l'échelle laboratoire uniquement, car jusqu'a maintenant on n'a pas eu des résultats qui nous permet de les appliqué à l'échelle utilisable ou industrielle mais les travaux continueront pour améliorer les conditions et optimiser les résultats.

Dans ce travail on a réalisée un système thermoélectrique solaire utilisons un concentrateur parabolique pour générer la chaleur nécessaire a alimenter le thermo générateur, et on a étudie l'influences des différents paramètres (la température, l'éclairement ….) sur le rendement de thermo générateur.

الملخص:

منذ قدم العصور اعتبر الغذاء والتدفئة حاجتين أساسيتين للإنسان، و عند اكتشافه النار و تعلمه التحكم بها بدأت رحلته في البحث عن الظروف الأحسن للحياة و بدء في تنويع إنتاج واستخدامات الطاقة الحرارية.

واحدة من استخدامات الطاقة الحرارية هي خاصية التحويل الحراري الكهربائي يسمح بتوليد الكهرباء من الحرارة المتاحة من خلال تحويل الأجهزة الحرارية (تأثيرSeebeck).

وتعتبر واحدة من الطرق البديلة لإنتاج الطاقة النظيفة، وقد تم إثبات فائدة مثل هاته الطريقة في توليد الطاقة الكهربائية في استعمالها في الفضاء الخارجي. وبالإضافة إلى هذه الجوانب تستخدم أيضا للتبريد (تأثير بلتي) في العديد من التطبيقات في مجال الالكترونيات.

هناك العديد من المصادر الحرارية المستخدمة في التحويل الكهربائي مثل حرارة الشمس، وزيت الوقود، والكتلة الحيوية و حرارة النفايات من مختلف الصناعات... الخ . ولا تزال هذه التطبيقات قيد الدراسة على مستوى المختبر فقط ذلك كان نتائج في هذا العمل قمنا بإنشاء نظام تحويل حراري كهربائي باستخدام مركز حراري لتوليد الحرارة اللازمة لتشغيل النظام.

وقمنا بدراسة تأثير عوامل مختلفة (درجة الحرارة والإشعاع ...) على أداء هذا النظام.

Acknowledgements

First of all Alhamdulillah, and thank to Allah whom without none of this work could've been done.
Thank you Allah for your blessings that can't be counted.

I would like to thank Mr. Said Nourredine for his support and guidance as my advisor throughout the duration of this Thesis project.

I would like to thank my parents for all the hard work and sacrifices they made for me throughout the years to make whom I am today.

I would like to thank my family, my friends, my colleagues and my dear ones for their everlasting support and encouragement , and for believing in me .

I would like to thank all my professors and all the department staff for the great working they're doing, and for helping all of us achieving our academic goals.

Thanks to the CDER for hosting me to do my experimental work and for the help they provided me with.

Last but not least I would like to thank everyone who helped me by any mean in my work, your help meant a lot to me.

List of figures

Nomenclature:

S1, S2: Seebeck coefficients

V: Voltage

A_a: Area of the collector aperture

A_r: The surface area of the receiver

A_w: The surface temperature of the cooling part is the total cooling area.

C: Area concentration ratio (geometric):

D_{hg} : The time difference (advance of 4 minutes per degree).

E_0: The useful electric

E : Equation of time, which is calculated by the equation (second):

$E_{r\to s}$: Exchange (view) factor

T_l : Local time (hours).

T_{sv}:(Hours) is the true solar time of the local studied

DT_l: Difference of local and standard time (hours).

T_0: The turbidity factor

T_1: The turbidity factor of absorption by atmospheric gases

T_2: The turbidity factor caused by aerosols

T_r: The temperature of the receiver,

$\overline{T}$: The average temperature of the heat sink,

$\dot{Q}_r$:The solar radiation incident

$\dot{Q}_L$: denotes the heat losses from the receiver plate

$\dot{Q}_{Lc}$: The total heat loss by natural convection

$\dot{Q}_{Lr}$: The total radiative heat loss from the receiver plate

$\dot{Q}_{in}$: The total radiation falling on the solar collector

$\dot{Q}_w$: The total heat is dissipated by the heat sink.

$\dot{Q}_d$: The unutilized heat dissipated from the cold side of the TEG

J: the day number of the year,

I_r: The averaged irradiance

I_a: The insolation incident on the collector aperture

I_b: The part of the incident sunlight

I: Direct flux

D: diffuse flux

G: Global flux

h: The height of the Sun (degrees)

h_a: is the convective heat transfer coefficient

Z: the altitude of the location (m)

δ: Solar declination

ω : The hour angle (degrees)

φ:(latitude degrees),

λ: longitude (degrees)

ψ : Azimuth of the sun (degrees)

ε: is the emissivity of the copper receiver plate

σ: is the Stefan–Boltzmann constant

η_h: The heat transfer efficiency can be evaluated as

η_0: Also, the overall efficiency in this case is given by

TEG: Thermoelectric generator

STEG: Solar Thermoelectric generator

Table of contents

Introduction:

Around 90% of the world's energy needs are satisfied by the fossil fuels such as oil and natural gas; however the rate which they are produced is significantly lower than the rate in which they are consumed. Furthermore, the combustion of fossil fuels produces carbon dioxide – the number one greenhouse gas – making the use of fossil fuels the leading cause of global warming. For this reason an economically and eco-friendly viable alternative is needed.

Solar energy has been proposed as a feasible renewable energy source, with the field dominated by photovoltaic and solar thermal power .Nevertheless, photovoltaic cells utilize only a small portion of radiation emitted by the sun (visible light) yet the entire spectrum of solar radiation may be converted into heat . Through the use of thermoelectric devices, this heat is then converted into electricity.

One of the biggest advantages of thermoelectric direct energy conversion from heat into electricity, eliminating the need for intermediate steps to obtain a usable output .

Solar thermal power has been slower to develop technologically and in a consumer market until recently.

In this work we propose to design , build and test a small-scale thermoelectric generator and the study of a concentrator Solar thermoelectric generator

This research proposes to design, build, and test a small-scale solar concentrator thermoelectric generator (STEG) to contribute to the further development of STEGs as a reasonable solar thermal energy source in a consumer market.

In the first chapter we talk briefly about the concept and the history of thermo electricity and thermoelectric generators and about the state of art and works presented in this field.

The second chapter presents the theoretical study in which we present and discuss the solar potential and the different models used to predict and calculate it.

Also we present the proprieties of the parabolic concentrator. and we perform a potential analysis of our proposed system.

In the third chapter we present the experimental analysis , the hardware design and the tests conducted .

Also we present and discuss the different obtained results.

I.1-Thermoelectricity:

Thermoelectricity is direct conversion of temperature differences to electric voltage and vice versa [1]. The main effects of thermoelectricity are:

I.1.1-The seebeck effect:

The Seebeck effect states that a voltage is induced when a temperature gradient is applied to the junctions of two differing materials [2].

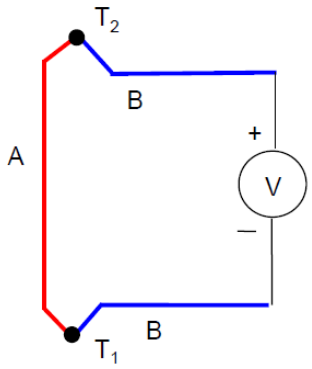

Figure 1: Seebeck effect schematic

$T2$ represents the absorber temperature, $T1$ represents the heat sink temperature, and the voltage difference is measured across a load or open circuit. The induced voltage V, is proportional to ΔT by the difference in the Seebeck coefficients of the two materials, as shown through the following equation

$$V = (S1 - S2)\,\Delta T$$

I.1.2-The peltier effect:

The Peltier Effect describes the inverse of the Seebeck's effect behavior, when an electrical current is passed through the junction of two differing materials; heat is either lost or absorbed at the junction according to the direction of the current [6].

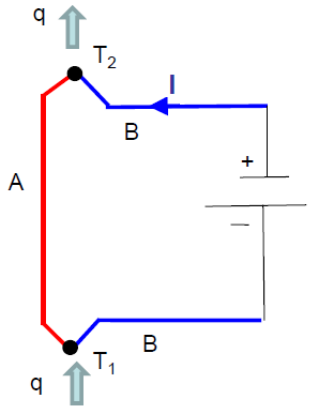

Figure 2: Peltier effect Schematic

The Peltier coefficient, π, demonstrates the proportionality between the heat flowing from a material due to a current and the current itself.

$$\pi = Q/I$$

I.1.3-The Thomson effect:

The physician William Thomson demonstrated that the Seebeck and the Peltier effects are related.

The Thomson effect defines the heat absorbed or released by time when an n electric current pass by a specific region of the matter with a gradient of temperature.

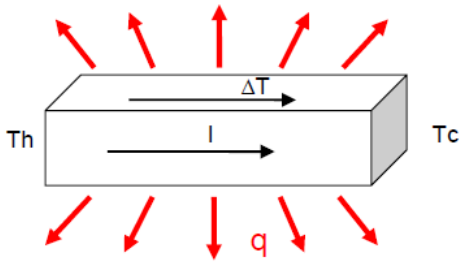

Figure 3: Thomson effect schematic

I.1.4-The Joule effect:

The circulation of the electric current across a resistive matter create a heat release.

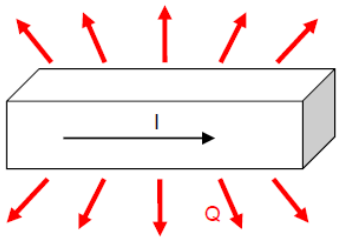

Figure 4: Joule effect schematic

I.2-History:

- **1794**: Alessandro Volta proved the existence of forces under the influence of temperature difference [3]. The experience he made is shown in figure 1.

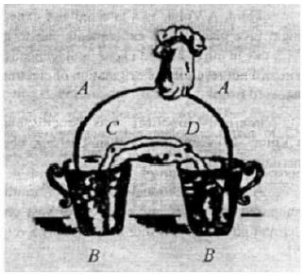

Figure 5: the experiment of Alexander Volta. A –metal arc (iron), B –glasses full of water, C ET D –parts of a frog immersed in water

- **1821:** Seebeck discovers that a circuit made from two dissimilar materials produced a voltage when their junctions were at different temperatures. It is later understood that a voltage will be induced in any material in a temperature gradient, known as the "Seebeck effect," which will be used to create thermoelectric power generators [4].

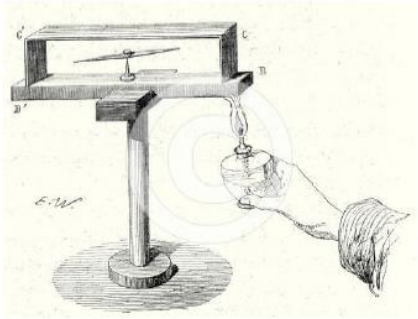

Figure 6: the original experiment of Thomas Johann Seebeck

- **1825:** Oersted gave correct explanations of Seebeck's experiments.

- **1834:** Jean Charles Athanase Peltier discovers that passing an electric current through two dissimilar materials produces heating or cooling at their junction. This is known as "Peltier effect," and will later be used to make refrigerators [5].
- **1854 :** William Thomson, also known as Lord Kelvin, finds that the Seebeck and Peltier effects are related, indicating that any thermoelectric material can be used to either generate power in a temperature gradient or pump heat with an applied current.

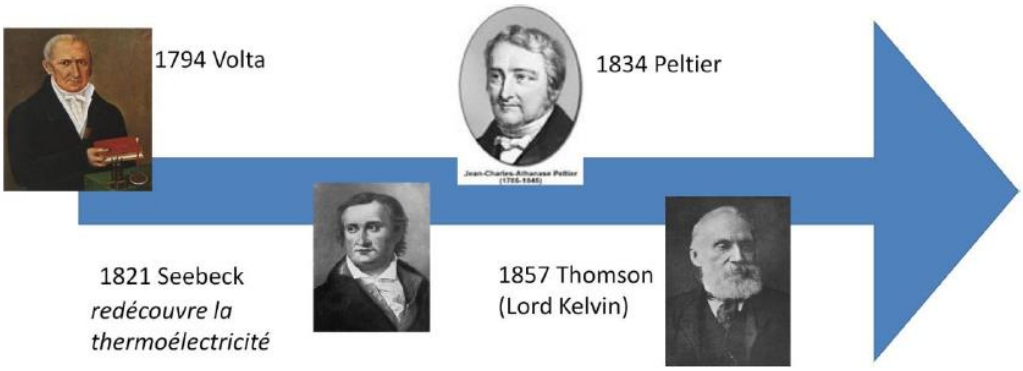

Figure 7 : Thermoelectric history line

- **1909-1911:** Altenkirch correctly derives the maximum efficiency of a thermoelectric generator (1909) and performance of a cooler (1911), which later developed into the 'thermoelectric figure of merit Z [6].

- **1928:** Ioffe begins to develop the modern theory of semiconductor physics in order to describe thermoelectric energy conversion. This opens up the understanding of how to engineer thermoelectric materials, as well as providing the basis for understanding the physics of transistors and microelectronics.

I.3-Thermoelectric generators:

Thermoelectric based power generation system is one of the viable candidates to generate electric power from heat energy. Thermoelectric devices are solid state devices [7] made from dissimilar n-type and p-type semiconductor materials called as thermo-elements. These devices provide maintenance free, reliable and light weight electric generators based on the Seebeck effect (direct conversion of temperature difference across thermo elements to the electric voltage) and coolers/heaters based on the Peltier effect (application of current across thermo elements resulting in heating/cooling of the junctions) [8].

A single thermo-element is form by two dissimilar materials, n-type and p-type semiconductors, which are connected electrically in series and thermally in parallel.
The conductor is generally made from copper due to its high thermal conductivity and low electrical resistivity, and the insulator is made from ceramic due to its low thermal resistance and insulation properties.
Heat is supplied on one side of TEG while the other end is maintained at a lower temperature by a heat sink.
As a result of the temperature difference, current will flow through an external load resistance. The power output depends on the temperature difference, the properties of the semiconductor materials and the external load resistance.
Each thermoelectric element is insulated, both electrically and thermally, from its surroundings, except at the junction to hot/cold reservoir contacts.
The internal irreversibility for the TEG is caused by Joule electrical resistive loss and heat conduction loss through the semiconductors between the hot and cold junctions and the external irreversibility is caused by finite rate heat transfers at the source and the sink [9].

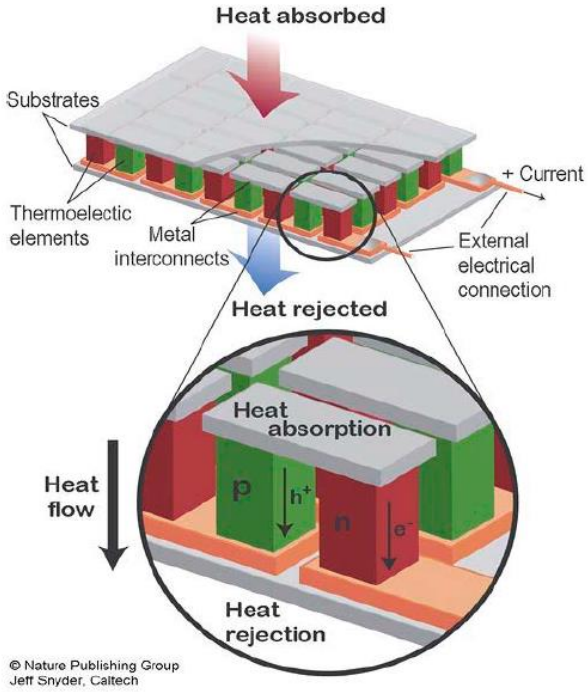

Figure 8: Thermoelectric Materials in a Thermoelectric Module [10]

I.4-The state of art:

The first concept for a STG was tested in 1922 by Coblentz for measuring infrared radiation from stars [11].Early works [12] showed low system efficiency (<1%), primarily due to low module ZT (<0.4), low solar concentration, and low hot-side temperature.

The pioneering research on STEGs for power generation was carried out by Maria Telkes 1947 [11]. By using a flat-plate collector covered with two glass panes and zinc-antimony alloys combined with negative bismuth alloys as thermoelectric materials, STEG efficiency reached 0.63% and was calculated to reach 1.05% if four panes of glass were to have been applied to the same device.

When optical concentration was applied to this system, the efficiency increased to 3.35%. In comparison, only 0.068% efficiency was reached with chromyl p-constantan thermoelectric materials in the flat-panel, two pane systems [13].

H. J. Goldsmid observed that, although metals and metal alloys have a high ratio of electrical to thermal conductivity, they have low thermoelectric power; yet semiconductors have a large enough thermoelectric power to compensate for their lower ratio of conductivities [14]. Thus, he applied this concept to the use of bismuth telluride semiconductors as thermoelectric materials in a STEG. He first built and tested a STEG with a flat plate absorber at low operating temperature, resulting in an overall efficiency under 1%. Trying again with a STEG equipped to operate at higher temperatures and utilizing a collector, Goldsmid again achieved lower efficiencies than expected (still less than 1%). Nevertheless, he noted that higher efficiencies are definitely possible if higher temperatures are achieved, one method of which is through the use of solar collectors [15].

Lately extensive research has been conducted on the thermoelectric generators for producing power from low grade (i.e. low temperature) heat particularly from the sun (Niu et al, 2009, Tundee et al, 2008, Pierre et al, 2008, Maneewana&Zeghmatib, 2007, Maneewan et al, 2003) [9].

Other researchers such as (Saitoh et al, 2006, Vatcharasathien et al, 2005, Omer & Infield, 2000) have utilized parabolic trough and compound parabolic concentrators to increase the intensity of the heat and thus temperature on the hot side of the TEG [9].

In 2010 Hongnan Fan et al, proposed electric an generator consists of parabolic dish collector of 1.8 m aperture diameter to concentrate sunlight on the receiver plate with 260 mm diameter, four BiTe based thermoelectric generators, heat transfer system to remove the waste heat from the thermoelectric cells, two-axis tracking system to follow the sun continuously during the day time and steel structural support to assemble components together and protect the system against wind loading. Experimental results show the system is able to produce electric power of up to 5.9W under the temperature difference across the thermoelectric cells of 35°C [9].

Inspired by Gang Chen's work and from his model, Sarah Watzman worked on increasing STEG efficiency using thermal concentration as opposed to optical concentration, eliminating the requirement for7 expensive equipment to track the sun in order to attain the necessary optical concentration to significantly increase the efficiency. Using a flat-panel solar absorber, solar radiation is collected, converted into heat, and concentrated onto the thermoelectric module.

Through the use of bismuth telluride thermoelectric materials and an evacuated system to

eliminate convective heat losses, Chen before her has achieved efficiencies of 4.6% - 5.2% and she reached only 0.03% [16].

M.Eswaramoorthy et al conducted an experimental study on small scale solar parabolic dish thermoelectric generator. The solar parabolic dish collector is fabricated using an unused satellite dish antenna fitted with polished aluminum sheet as concentrator surface. Thermoelectric generator consists of commercial thermoelectric modules embedded between the receiver plate and water cooled heat sink which is placed on the focal plane of manual tracking parabolic dish collector [17].

II.1-Solar Potential:

II.1.1-THE SUN:

The sun is a sphere of intensely hot gaseous matter with a diameter of 1.39 × 109 m and is, on the average, 1.5 × 1011 m from the earth. As seen from the earth, the sun rotates on its axis about once every 4 weeks. However, it does not rotate as a solid body; the equator takes about 27 days and the Polar Regions take about 30 days for each rotation. The sun has an effective blackbody temperature of 5777 K.1 The temperature in the central interior regions is variously estimated at 8 × 106 to 40 × 106 K and the density is estimated to be about 100 times that of water. The sun is, in effect, a continuous fusion reactor with its constituent gases as the ‘‘containing vessel’’ retained by gravitational forces. Several fusion reactions have been suggested to supply the energy radiated by the sun. The one considered the most important is a process in which hydrogen (i.e., four protons) combines to form helium (i.e., one helium nucleus); the mass of the helium nucleus is less than that of the four protons, mass having been lost in the reaction and converted to energy.

The energy produced in the interior of the solar sphere at temperatures of many millions of degrees must be transferred out to the surface and then be radiated into space. A succession of radiative and convective processes occur with successive emission, absorption, and reradiation; the radiation in the sun’s core is in the x-ray and gamma-ray parts of the spectrum, with the wavelengths of the radiation increasing as the temperature drops at larger radial distances [18].

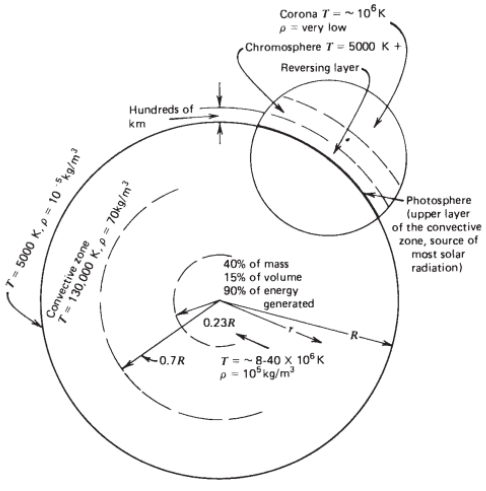

Figure 9: The structure of the sun [18]

II.1.2-Earth-Sun distance:

The trajectory of the Earth around the Sun is an ellipse with Sun at one of the foci. The mean Earth-Sun distance varies from 144 (21 December) to 154 million Km (21 June) [19, 20]. The correction coefficient of the Earth-Sun distance (dimensionless) can be calculated by the equation [19, 20]:

$$c_t = 1 + 0.034.\cos(j - 2) \quad \text{(II.1)}$$

Where *J* is the day number of the year, ranging from 1 on 1 January to 365 on 31December.

II.1.3- Solar declination:

the solar declination δ (degrees) is the angle between the direction of the Sun with the equatorial plane of the Earth [21]. The declination varies from-23°27' at the winter solstice to +23°27' at the summer solstice, while at the equinoxes is zero [19]. The solar declination can be calculated by the equation given by Copeer (1967):

$$\delta = 23.25.\sin(0.986.(j + 284)) \quad \text{(II.2)}$$

II.1.4- Hour Angle:

The hour angle ω (degrees) is the angle between the meridian plane passing through the center of the Sun and the vertical plane of the place (meridian) and defines the true solar timeT_{sv}(hours) [22]. The hour angle can be calculated by the next equation [23, 24]:

$$\omega = 15.(12 - T_{sv}) \quad \text{(II.3)}$$

With T_{sv}(hours) is the true solar time of the local studied and it is determined by the relationship:

$$T_{sv} = T_l - DT_l + (D_{hg} + {}^{E}/_{60})/60 \quad \text{(II.4)}$$

•T_l : local time (hours).

•DT_l: Difference of local and standard time (hours).

•D_{hg} : the time difference (advance of 4 minutes per degree).

• E : equation of time, which is calculated by the equation (second):

$$E = 45.8.\sin\left({}^{2.\pi.j}/_{365} - 0.026903\right) + 595.4.\sin\left({}^{4.\pi.j}/_{365} + 0.352835\right) \quad \text{(II.5)}$$

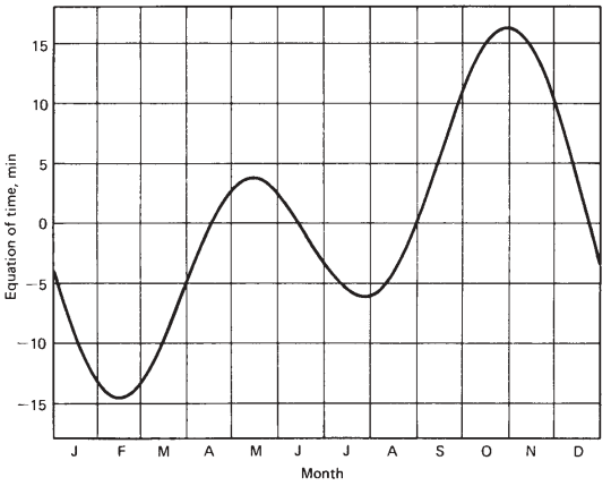

Figure 10: The equation of time *E* in minutes as a function of time of year.

II.1.5- Geographical coordinates:

The geographical coordinates of the studied location are represented by the latitude φ(degrees), longitude (degrees) and altitude h or z (m), where the latitude is the angle between the position study with the equator and longitude is the angle between the meridian of the study with the meridian position [19].

II.1.5.1- Height of the Sun:

The height of the Sun h (degrees) is the angle between the horizontal planes with the direction of the Sun. The value h=0is at sunrise and sunset, The Height of the Sun varies between 90 ° (zenith) and -90 ° (nadir) [22] and it is calculated by the following formula:

$$h = sin^{-1}.(sin(\varphi).\sin(\delta) + \cos(\varphi).\cos(\delta).\cos(\omega)) \quad \text{(II.6)}$$

II.1.5.2- Azimuth of the Sun:

The azimuth of the sun ψ (degrees) is the angle on the horizontal plane, being the projection of the direction of the Sun with the direction to the south. The azimuth is between -180 ≤ ψ ≤ 180 ° [21], and it is a function of the solar declination δ, Height of the Sun h and hour angle ω, can be calculated by the next formula:

$$\psi = sin^{-1}(\cos(\delta).\frac{\sin(\omega)}{\cos(h)}) \quad \text{(II.7)}$$

II.1.5.3- Day length:

it is calculated by the following formula [22]:

$$S_j = 24(1 - \frac{cos^{-1}(\tan(\delta).\tan(\lambda))}{\pi} \quad \text{(II.8)}$$

It is expressed in hours.

II.1.5.4- Sunshine duration:

it is calculated by the following formula [22]:

$$S_g = \frac{2}{15}.cos^{-1}(-\tan(\varphi).\tan(\delta)) \quad \text{(II.9)}$$

It is expressed in hours.

II.1.2-DEFINITIONS:

Air Mass *m* the ratio of the mass of atmosphere through which beam radiation passes to the mass it would pass through if the sun were at the zenith [18].

Beam Radiation The solar radiation received from the sun without having been scattered by the atmosphere. (Beam radiation is often referred to as direct solar radiation; to avoid confusion between subscripts for direct and diffuse; we use the term beam radiation.) [18].

Diffuse Radiation The solar radiation received from the sun after its direction has been changed by scattering by the atmosphere. (Diffuse radiation is referred to in some meteorological literature as sky radiation or solar sky radiation; the definition used here will distinguish the diffuse solar radiation from infrared radiation emitted by the atmosphere.) [18].

Total Solar Radiation The sum of the beam and the diffuse solar radiation on a surface.4 (The most common measurements of solar radiation are total radiation on a horizontal surface, often referred to as **global radiation** on the surface.) [18].

Irradiance, W/m² the rate at which radiant energy is incident on a surface per unit area of surface. The symbol *G* is used for solar irradiance, with appropriate subscripts for beam, diffuse, or spectral radiation [18].

Irradiation or **Radiant Exposure**, J/m2 the incident energy per unit area on a surface, found by integration of irradiance over a specified time, usually an hour or a day [18].

Insolation is a term applying specifically to solar energy irradiation. The symbol *H* is used for Insolation for a day. The symbol *I* is used for Insolation for an hour (or other period if specified). The symbols *H* and *I* can represent beam, diffuse, or total and can be on surfaces of any orientation.

Subscripts on *G*, *H*, and *I* are as follows: *o* refers to radiation above the earth's atmosphere, referred to as extraterrestrial radiation; *b* and *d* refer to beam and diffuse radiation; *T* and *n* refer to radiation on a tilted plane and on a plane normal to the direction of propagation. If neither *T* nor *n* appears, the radiation is on a horizontal plane [18].

Radiosity or **Radiant Existence**, W/m² the rate at which radiant energy leaves a surface per unit area by combined emission, reflection, and transmission [18].

Emissive Power or **Radiant Self-Existence**, W/m² the rate at which radiant energy leaves a surface per unit area by emission only [18].

II.1.3-Radiation calculation models:

To predict the daily direct, diffuse and global solar radiation data many models have been developed. We will be demonstrating some of these models which are (The Cooper and Perrin Brichambaut Models, and The Capderou Model).

We dedicate this respectful radiation respectively by the letters I (direct), D (diffuse) and G (global), all these are calculated with$W.m^{-1}$.

II.1.3.1-The Cooper and Perrin of Brichambaut Models:

The Cooper model [25] calculates the solar flues (Cooper 1992) as:

• the direct flux can be calculated by:

$$I = I_0.\sin(h) \quad \text{(II.10)}$$

• The diffuse flux can be calculated by:

$$D = 125.(\sin(h))^{0.4} \quad \text{(II.11)}$$

• the global flux can be calculated by:

$$G = I + D \quad \text{(II.12)}$$

More specifically, in Perrin brichambaut model [25, 26], the above relationships are transformed into the following ones according to the atmospheric conditions and climatic conditions:

• Areas with air pollution:

- Direct flux:

$$I_{min} = 1260.\exp(-\frac{2.23}{4.\sin(h+1)}) \quad \text{(II.13)}$$

- Diffuse flux :

$$D_{min} = 166.67.(\sin(h))^{0.4} \quad \text{(II.14)}$$

- Global flux :

$$G_{min} = 955.(\sin(h))^{1.25} \quad \text{(II.15)}$$

• Normal conditions :

- Direct flux:

$$I_{mean} = 1230.\exp(-\frac{1}{2.5.\sin(h+1.6)}) \quad \text{(II.16)}$$

- Diffuse flux :

$$D_{mean} = 125.(\sin(h))^{0.4} \quad \text{(II.17)}$$

- Global flux:

$$G_{mean} = 1080.(\sin(h))^{1.22} \quad \text{(II.18)}$$

• Clear Skies:

- Direct flux:

$$I_{max} = 1210.\exp(-\frac{1}{6\sin(h+1)}) \quad \text{(II.19)}$$

- Diffuse flux:

$$D_{max} = 93.75.(\sin(h))^{0.4} \quad \text{(II.20)}$$

- Global flux:

$$G_{max} = 1130.(\sin(h))^{1.15} \quad \text{(II.21)}$$

II.1.3.2-The Capderou Model:

The Capderou model [21] uses the atmospheric turbidity to calculate the direct and diffuse components of solar radiation received on horizontal plane.

The absorption and diffusion caused by the atmospheric constituents can be expressed by turbidity factors [27]; the knowledge the atmospheric turbidity factor refers to determine the solar radiation for clear skies.

The most commonly used is the Link turbidity factor, which for clear skies is given by [28]:

$$T_L = T_0 + T_1 + T_2 \quad \text{(II.22)}$$

With T_0(dimensionless) is the turbidity factor the gaseous absorption [29]. The modeling of this factor based only on geo-astronomical parameters, is given by the following expression:

$$T_0 = 2.4 - 0.9\sin(\varphi) + 0.1(2 + \sin(\varphi))A_{he} - 0.2\,Z - (1.22 + 0.14A_{he})(1 - \sin(h)) \quad \text{(II.23)}$$

T_1 : (Dimensionless) is the turbidity factor of absorption by atmospheric gases [29] ($CO_2O_2O_3$), can be calculated by the formula:

$$T_1 = 0.89^z \quad \text{(II.24)}$$

T_2 : (Dimensionless) is the turbidity factor caused by aerosols [29], and can be calculated by the formula:

$$T_2 = (0.9 + 0.4A_{he}).(0.63)^z \quad \text{(II.25)}$$

With Z (m) is the altitude of the location [21]:

We set:

$$A_{he} = \sin(\left(\frac{360}{365}\right).(j - 121)) \quad \text{(II.26)}$$

Direct solar radiation:

It can be calculated by the formula [27]:

$$I_b = I_0.C_t.\exp\left(-T_L.\left(0.9 + \frac{9.4\sin(h)}{T_1}\right)^{-1}\right).\sin(h) \quad \text{(II.27)}$$

Diffuse solar radiation:

It can be calculated by the formula [27]:

$$D = I_0.C_t.\exp(-1 + \log(\sin(h)) + a + \sqrt{a^2 + b^2} \quad \text{(II.28)}$$

With:

$$a = 1.1 \;\; ; \;\; b = \log(T_L - T_0) - 2.8 + 1.02.(1 - \sin(h))^2 \quad \text{(II.29)}$$

Globalesolar radiation:

It is the sum of the direct and diffuse solar radiation [27]:

$$\mathrm{G} = \mathrm{I_b} + \mathrm{D} \quad \text{(II.30)}$$

II.1.4-A comparative study:

To validate the solar radiation results obtained by the Capderou model, we'll confront some values of the solar radiation provided by the meteorological station of the research center (U.D.E.S) of Bousmail, Tipaza, northern Algeria (Latitude: 36.642, Longitude: 2.696, Altitude: 55 meters), with values on the normal plane calculated by Matlab.

II.1.4.1-The Measuring Instrumentations:

The measurement of global and diffuse radiations at ground was performed by: A pyranometer (global solar radiation). This instrument measures the radiation incident on horizontal surface blackened from a solid angle of 2π steradians. The spectral range covers wave lengths from 0.3 to 3 μm. The received radiation is converted to heat by the blackened surface. The temperature difference between the surface and the body of the instrument is proportional to the irradiance of the global radiation; it is measured by a thermopile consisting of several thermocouples connected in series [30].

A similar pyranometer (diffuse solar radiation) having an added shades band obscure the direct radiation. Depending on circumstances, this screen may be either a disc or a sphere [30].
The value of the direct radiation is obtained later by the difference of the global and the diffuse radiations.

Figure 11: Pyranometer

Figure 12: Similar Pyranometer

The following figures present the comparative graphs of the direct and global radiations by the Capderou model, with the experimental data of the site.

We'll use the instant relative error expression:

$$E_{r_r} = \frac{|G_{measured} - G_{calculated}|}{G_{measured}}$$

G: solar radiation (Wm^{-2})

to evaluate the error between the results.

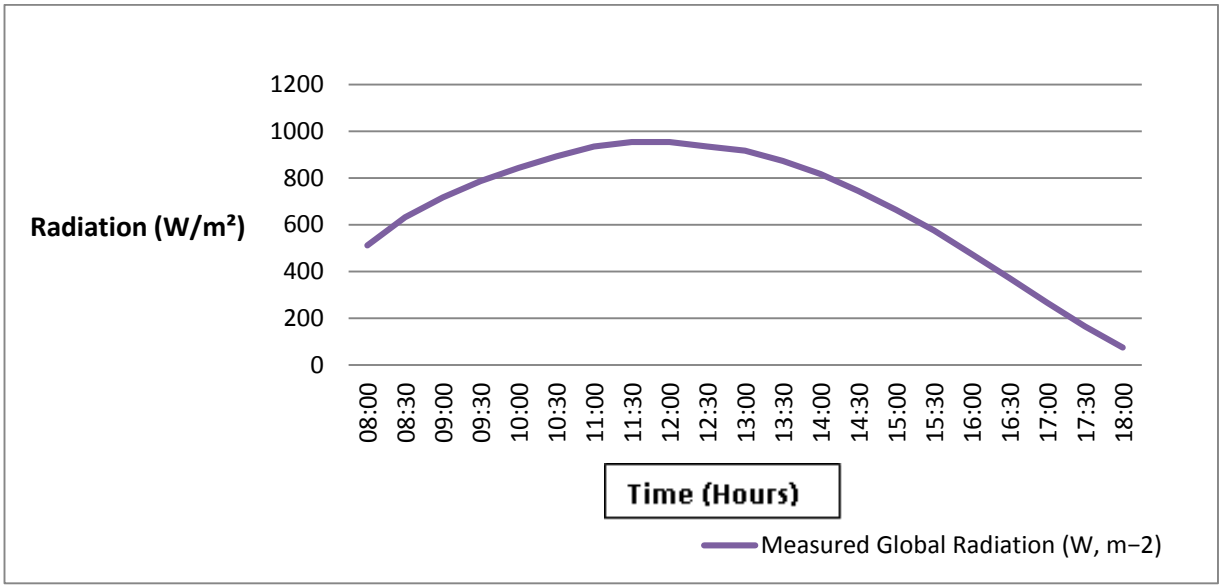

Figure 13: Measured global radiation (03/05/2016)

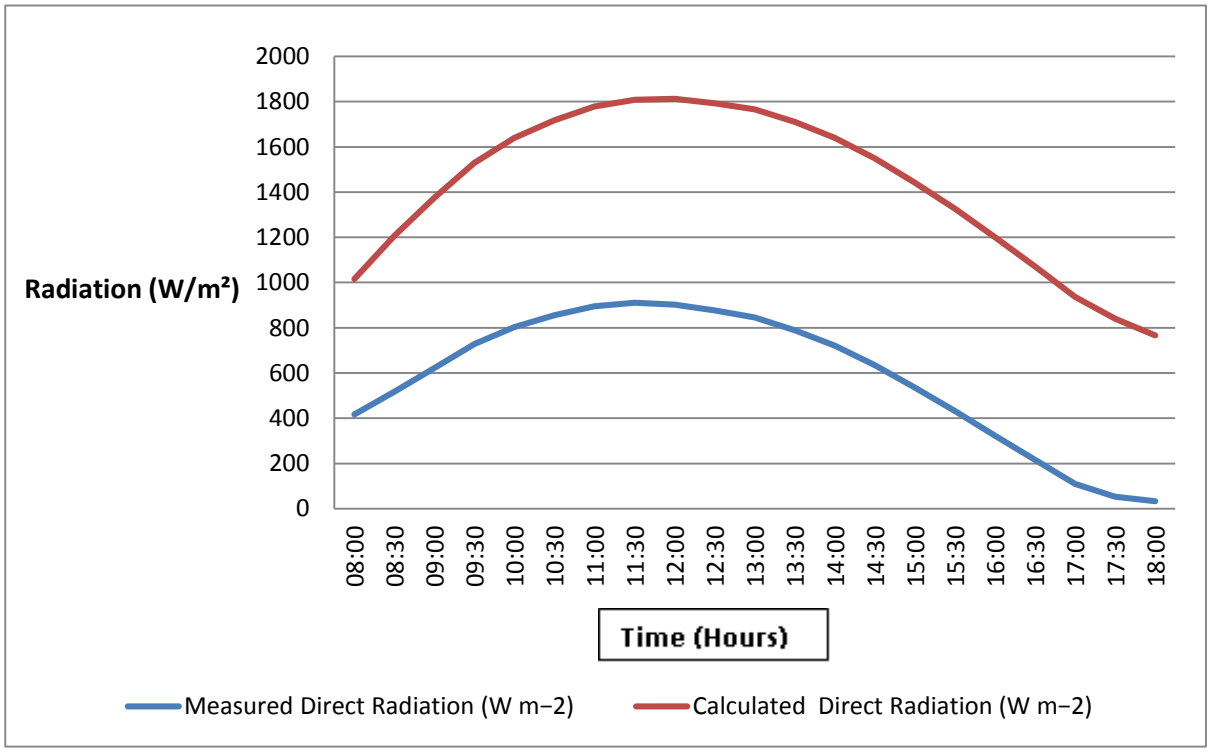

Figure 14: Comparison between the measured and the calculated direct radiation (03/05/2016)

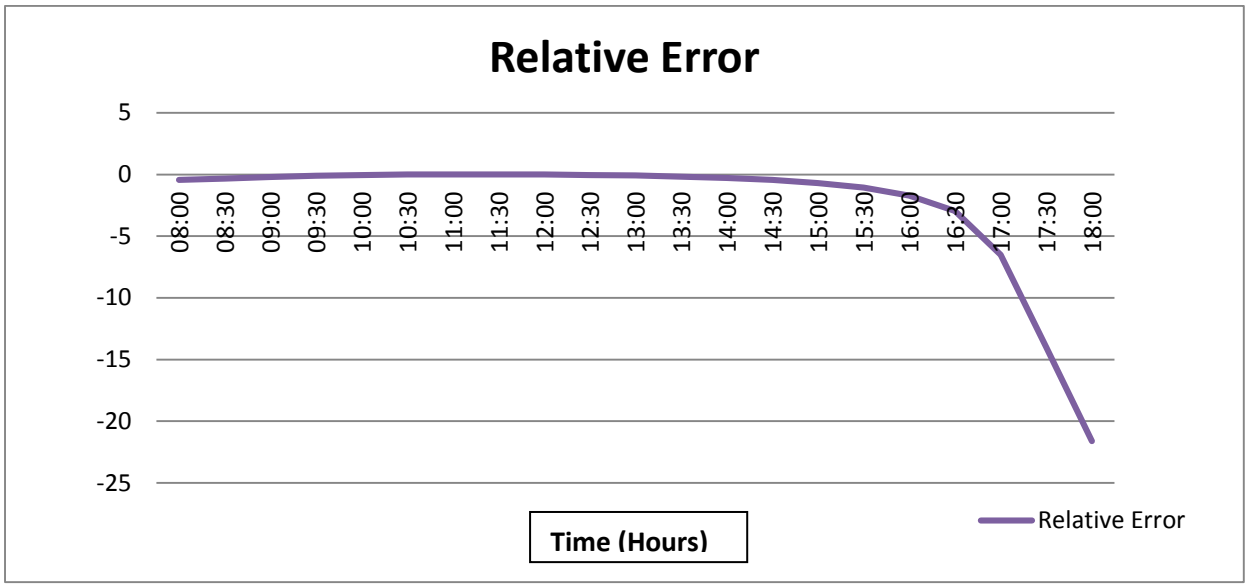

Figure 15: The instant relative error between measured and calculated direct radiation (03/05/2016)

According to the figures drawn previously it can be seen that the direct solar flue estimated by the Capderou model is super imposed with that measured by the Bousmail research center station.

II.2-The concentrator:

Concentrating, or focusing, collectors intercept direct radiation over a large area and focus it onto a small absorber area. These collectors can provide high temperatures more efficiently than flat-plate collectors, since the absorption surface area is much smaller. However, diffused sky radiation cannot be focused onto the absorber. Most concentrating collectors require mechanical equipment that constantly orients the collectors toward the sun and keeps the absorber at the point of focus. Therefore; there are many types of concentrating collectors [31].

There are four basic types of concentrating collectors [31].

- Parabolic trough system
- Parabolic dish
- Power tower
- Stationary concentrating collectors

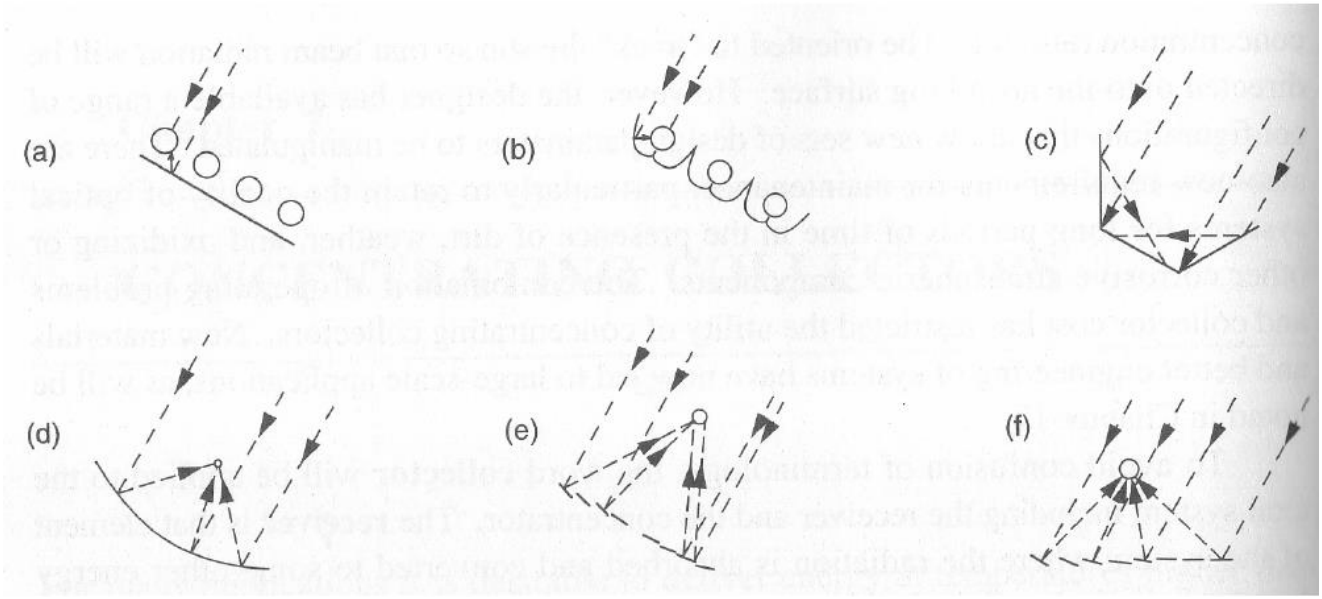

Figure 16: Different concentrating collectors

a) Tubular absorbers with diffusive back reflector;
b) Tubular absorbers with specular cusp reflector;
c) Plane receiver with plane reflector;
d) Parabolic concentrator;
e) Fresnel reflector
f) Array of heliostats with central receiver

II.2.1-Concentration Types [32]:

- Planar and non-concentrating type which provides concentration ratios of up to four and are of the flat plate type.
- Line focusing type produces a high density of radiation on a line at the focus. Cylindrical parabolic concentrators are of this type and they could produce concentration ratios of up to ten.

- Point focusing type generally produces much higher density of radiation in the vicinity of a point. Paraboloids are examples of point focus concentrators.

II.2.2-Concentration Ratio :

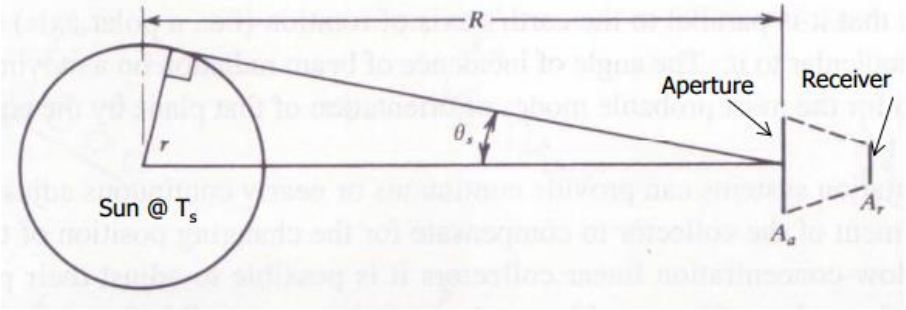

Figure 17: concentrating ratio schematic

- Area concentration ratio (geometric):

  The area of the collector aperture A_a divided by the surface area of the receiverA_r [32].

$$C = \frac{A_a}{A_r} \tag{II.31}$$

- Optical concentration ratio:

  The averaged irradiance (radiant flux) (I_r) integrated over the receiver area (A_r), divided by the Insolation incident on the collector aperture [32].

$$C_0 = \frac{\frac{1}{A_r}\int I_r . d . A_r}{I_a} \tag{II.32}$$

I_r is the averaged irradiance

I_a is the insolation incident on the collector aperture

II.2.3-Radiative Heat Exchange between the Sun and the Receiver:

The sun is assumed to be a blackbody at Ts and the radiation from the sun on the aperture/receiver is the fraction of the radiation emitted by the sun which is intercepted by the aperture [32].

$$Q_{s\to r} = A_a.\frac{r^2}{R^2}.\sigma.T_s{}^4 \quad \text{(II.33)}$$

$$\sigma = 5.6697 * 10^{-8}\ W/m^4K^4 \quad \text{(II.34)}$$

A perfect receiver, such as a blackbody, radiates energy equal to ArTr4 and a fraction of this reaches the sun

$$Q_{r\to s} = A_r.\sigma.T_r{}^4.E_{r\to s} \quad \text{(II.35)}$$

$E_{r\to s}$: Exchange (view) factor

II.2.4-Parabolic concentrator:

A parabolic dish collector is similar in appearance to a large satellite dish, but has mirror-like reflectors and an absorber at the focal point. It uses a dual axis sun tracker [31].

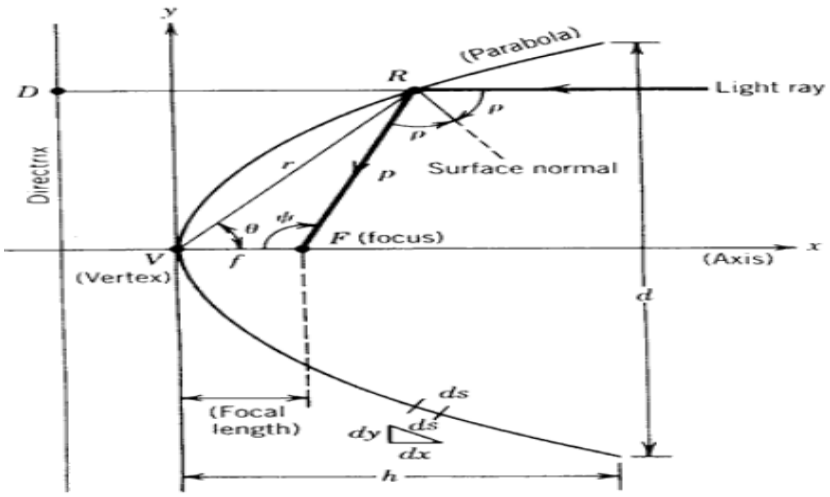

Figure 18: The parabola

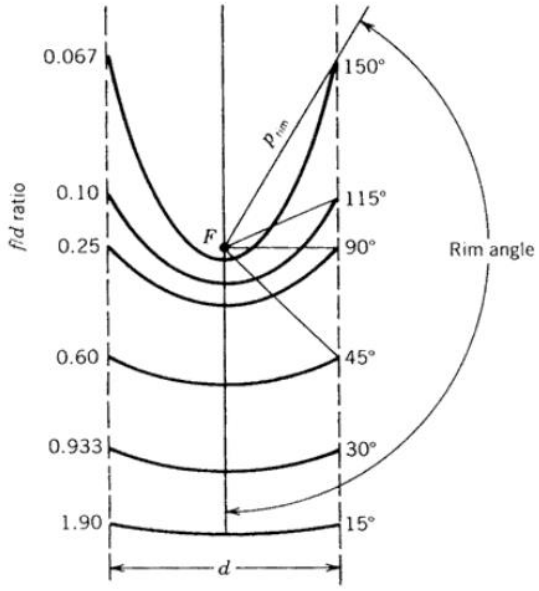

Figure 19: Segments of a parabola having a common focus *F* and the same aperture diameter.

If the incident beam of parallel rays is even slightly off normal to the mirror aperture, beam dispersion occurs, resulting in spreading of the image at the focal point. For a parabolic mirror to focus sharply, therefore, it must accurately track the motion of the sun to keep the axis (or plane) of symmetry parallel to the incident rays of the sun.

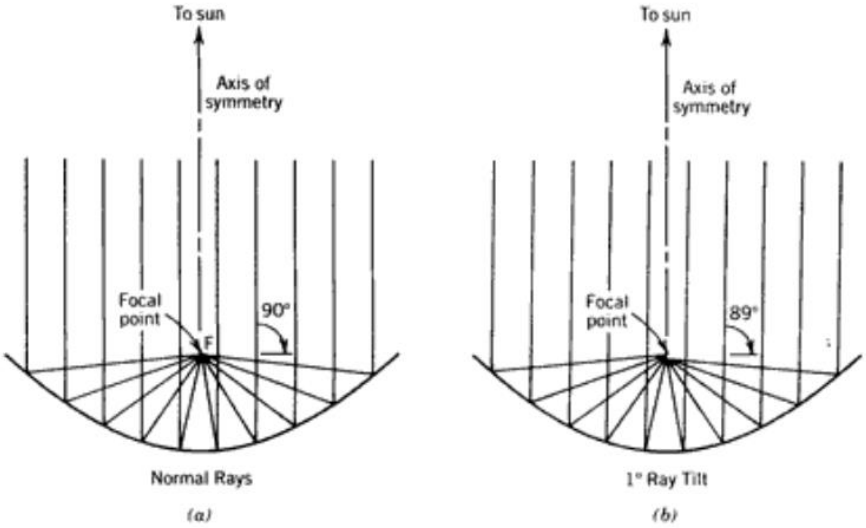

Figure 20: Demonstration of beam dispersion

The prototype we used was an offset or off-axis parabolic dish type (RCA 18" dish). This offset parabolic concentrator, sometimes called Scheffler collector, is a three dimensional dish shaped structure in which the focus point is located outside the collector area.

An offset-feed dish antenna has a reflector which is a section of a normal parabolic reflector. If the section does not include the center of the dish, then none of the radiated beam is blocked by the feed antenna and support structure [33].
Otherwise, only a small bit at the edge of the beam is blocked. For small dishes, feed blockage in an axial-feed dish causes a significant loss in efficiency. Thus, we might expect an offset-feed dish to have higher efficiency than a conventional dish of the same aperture [33].

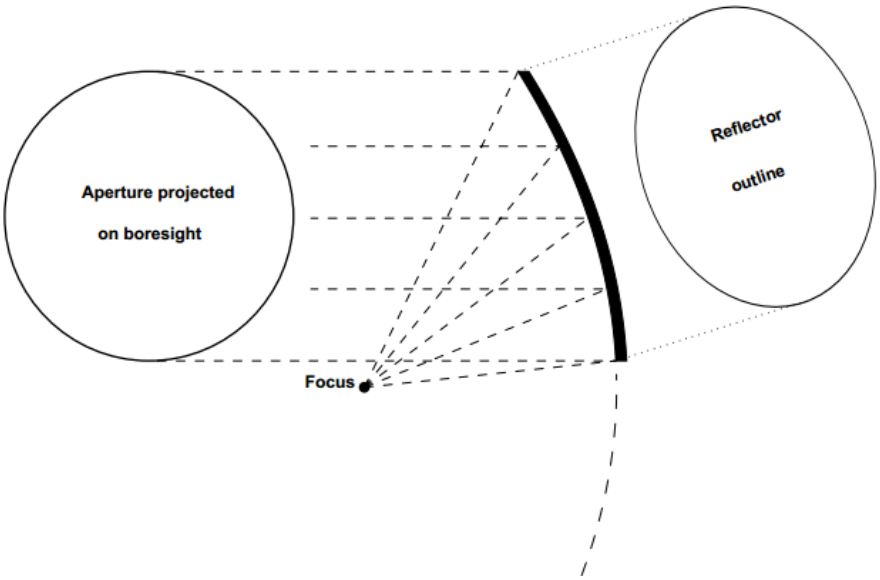

Figure 21: Geometry of Offset parabolic dish Antenna

II.2.5-Measurements and Calculation for an Offset Parabolic Reflector:

The geometry of an offset-feed dish antenna is a bit more complicated than a conventional dish antenna, but the measurements needed to use one are straight forward. We need to first determine the tilt angle of the reflector, then do some curve fitting calculations for the dish surface, calculate the focal length, and finally determine the focal point in relation to the offset reflector [33].

One common type of offset parabolic reflector has an oval shape, with a long axis from top to bottom and a shorter axis from side to side. However, if you were in the beam of this antenna, looking down the bore sight, it would appear to be circular, with the feed at the bottom. Tilt the top of the reflector forward, until it appears circular from a distance, and it will be in the correct orientation to operate with the beam on the horizon [33].

The approximate tilt can be determined much more accurately with a simple calculation:
Tilt angle (from horizontal) = *arcsin* (short axis / long axis)
For the RCA 18” dish, the short axis is 460 mm. (about 18”) and the long axis is 500 mm.
Therefore, the tilt angle = *arcsin* (460/500) = 66.9 degrees above horizontal.

[Note: the *arcsin* function is called *sin*-**1** on some scientific calculators]
one millimeter is sufficiently accurate for most dish dimensions, so using millimeters for calculations eliminates a lot of tedious decimals.

If the offset reflector is not oval, we can still use the same calculation by placing it on the ground with the reflecting surface upward and filling it with water.
The surface of the water in the dish should be an oval just touching the top and bottom rims, the other axis of the oval of water is the shorter axis.
The other dimension we need is location and depth of the deepest point in the dish. The deepest point is probably not at the center, but somewhere along the long axis. Using a straight edge across the rim for an oval dish, or the water depth for other shapes, locate the deepest point and measure its depth and distance from the bottom edge on the long axis.
For the RCA dish, the deepest point is 43 mm deep at 228 mm from the bottom edge on the long axis [33].
When the dish is tilted forward to 66.9 degrees above horizontal, the translated coordinates describe the curve of the long axis by three points:

0, 0 mm (bottom edge)

49.8, 226.6 mm (deepest point)

196, 460 mm (top edge)

If we assume that the bottom edge is not at the axial center of a full parabola of rotation(the equivalent conventional dish of which the offset dish is a section), but rather is offset from the center by an amount X0, Y0, then all three points must fit the equation:

$$4 * f * (x + x_0) = (y + y_0)^2 \qquad \text{(II.36)}$$

The unknowns are x_0, and y_0, and f, the focal length; plugging in the three points gives us 3 equations and 3 unknowns, a readily soluble 3x3 matrix (actually, the 0,0 point allows reduction to a 2x2 matrix, even easier, followed by a simple calculation for x_0 and y_0).
Version 2 of the HDL_ANT program will do the calculations for you.
For the RCA dish, the answers are:

$$f = 282.8mm = 11.13"$$

x_0 = 0.1 mm behind bottom edge

y_0 = 11 mm below bottom edge, so the feed doesn't block the aperture at all.

However, the bottom edge of the dish should be at the center of the full parabola, so that

x_0= 0 and y_0 = 0.

We can repeat the calculations above with slightly different tilt angles until x_0 = 0 and y_0 = 0; for the RCA dish, the new tilt angle is 68.3°, a small change from our original estimate of 66.9°. The focal length is then calculated to be 291mm [33].

So, we tilt the dish to 68.3 degrees from horizontal, and the feed is on a line level with the bottom edge of the dish. To help locate the focal point, it is 291 mm from the bottom edge, and 476 mm from the top edge, both edges on the long axis [33].

For the RCA dish, we can also calculate the illumination angle to be 77.2 degrees on the long axis and 78.1 degrees on the short axis, so it is roughly symmetrical. The optimum feed for this illumination angle is equivalent to an axial-feed dish with ***f*/D** ≅ 0.71 [33].

Although the illumination angles I equivalent to an ***f*/D** ≅ 0.71, the surface is a section of a parabola about 36.5 inches in diameter with a focal length of about 11.5 inches. Thus, the real ***f*/D** is 0.31, so the focal distance is quite critical [33].

(Note: the **HDL_ANT** can perform all the calculations required.)

II.3-Performance analysis:

II.3.1-Thermal Efficiency of the Dish System:

We formulate the following analytical model to assess the thermal and electrical performance of the module under different experimental conditions.
Figure 22 presents a schematic of the dish collector with only the alliminum receiver plate assembled at the dish focal point. The incoming solar radiation incident on the receiver plate is

$$\dot{Q}_r = A_c \mathfrak{y}_r I_b \quad \text{(II.37)}$$

where A_c is the area of the solar collector (or reflector) and $\mathfrak{y}_r$is the reflectance of the material, which is dependent on the type of reflective material used (being 60% for chrome paint), surface condition (highly polished), the uniformity of the coating, and the accuracy of the reflector profile.

I_b Is the part of the incident sunlight per unit area (I) that can be successfully converged by the collector as a beam onto the receiver plate

$$I_b = I - I_d \quad \text{(II.38)}$$

Where I_d is the diffuse component of radiation which is not utilized by the concentrator . The fraction of incident sunlight directed into the beam is primarily dependent on atmospheric conditions, normally being above 90% for a clear sky. It should be noted that the fraction of I_b incident on the receiver plate is also dependent on the accuracy of the tracking system.

I_b can be measured by using a pyranometer.

The standard value of b at noon for a clear sky is 1000 W/m².

As illustrated in Fig. 22, the energy balance for the system can be expressed as:

$$\dot{Q}_r = \dot{Q}_L \quad \text{(II.39)}$$

where $\dot{Q}_r$ is the solar radiation incident on the receiver (the copper plate) and $\dot{Q}_L$ denotes the heat losses from the receiver plate to the surroundings.

In other words, the total radiation that can be by the receiver should be equal to the overall heat loss by both natural convective and radiative loss.

Therefore, the equation can also be presented as:

$$A_c \eta_r I_b = \dot{Q}_{Lc} + \dot{Q}_{Lr} \quad \text{(II.40)}$$

where $\dot{Q}_{Lc}$ is the total heat loss by natural convection, which can be obtained using

$$\dot{Q}_{Lc} = 2A_r h_a (T_r - T_a) \quad \text{(II.41)}$$

where T_r is the temperature of the receiver, $A_r$is the area of the receiver, h_a is the convective heat transfer coefficient (5.7 + 3.8Vw, where Vw is the wind velocity in m/s) and, T_a is the ambient temperature.

Furthermore, $\dot{Q}_{Lr}$ is the total radiative heat loss from the receiver plate, which can be obtained using .

$$\dot{Q}_{Lr} = 2A_r \varepsilon \sigma \left({T_r}^4 - {T_a}^4 \right) \quad \text{(II.42)}$$

where ε is the emissivity of the copper receiver plate (0.8) and σ is the Stefan–Boltzmann constant (5.67 9 108 W/m²/K4).

In practice, it is hard to obtain the exact balance in Eq. (4) due to experimental errors not accounted for in the analysis. Therefore, herein, the overall efficiency, go, is introduced as an assessment parameter to determine the capacity and efficiency of the dish, being obtained as

$$\eta_0 = \frac{\dot{Q}_{Lc} + \dot{Q}_{Lr}}{\dot{Q}_{in}} \quad \text{(II.43)}$$

where $\dot{Q}_{in}$ is the total radiation falling on the solar collector:

$$\dot{Q}_{in} = A_c \times I_b \quad \text{(II.44)}$$

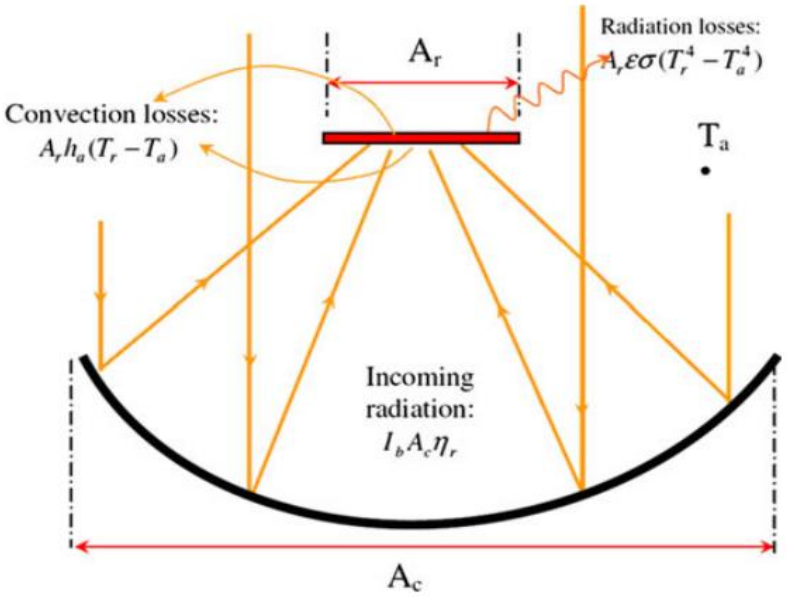

Figure 22: Schematic of the heat flow in the single-dish system

II.3.2-Thermal Efficiency of the Heat Transfer System:

Figure 23 shows a schematic of the dish system with a cooling module attached to the surface of the receiver. Solar radiation is concentrated onto the receiver plate by the dish, generating heat that is finally dissipated by the micro channel heat sink.
The energy balance equation is:

$$A_c \eta_r I_b = \dot{Q}_{Lc} + \dot{Q}_{Lr} + \dot{Q}_w \qquad \text{(II.45)}$$

where $\dot{Q}_w$the total heat is dissipated by the heat sink.

Furthermore, natural convection as well as radiative loss from the cooling area should also be taken into account when calculating the total heat losses.
Therefore, Eqs. (41) And (42) in this case become:

$$\dot{Q}_{Lc} = h_a A_w(\overline{T} - T_a) + h_a A_c(T_r - T_a) \qquad \text{(II.46)}$$

$$\dot{Q}_{Lr} = A_w \varepsilon \sigma \left(\bar{T}^4 - {T_a}^4\right) + A_c \varepsilon \sigma \left({T_r}^4 - {T_a}^4\right) \quad \text{(II.47)}$$

Where $\bar{T}$ is the average temperature of the heat sink, being the surface temperature of the cooling part, A_w is the total cooling area.

The heat transfer efficiency can be evaluated as:

$$\eta_h = \frac{\dot{Q}_w}{\dot{Q}_{in}} \quad \text{(II.48)}$$

Also, the overall efficiency in this case is given by:

$$\eta_0 = \frac{\dot{Q}_w + \dot{Q}_{Lc} + \dot{Q}_{Lr}}{\dot{Q}_{in}} \quad \text{(II.49)}$$

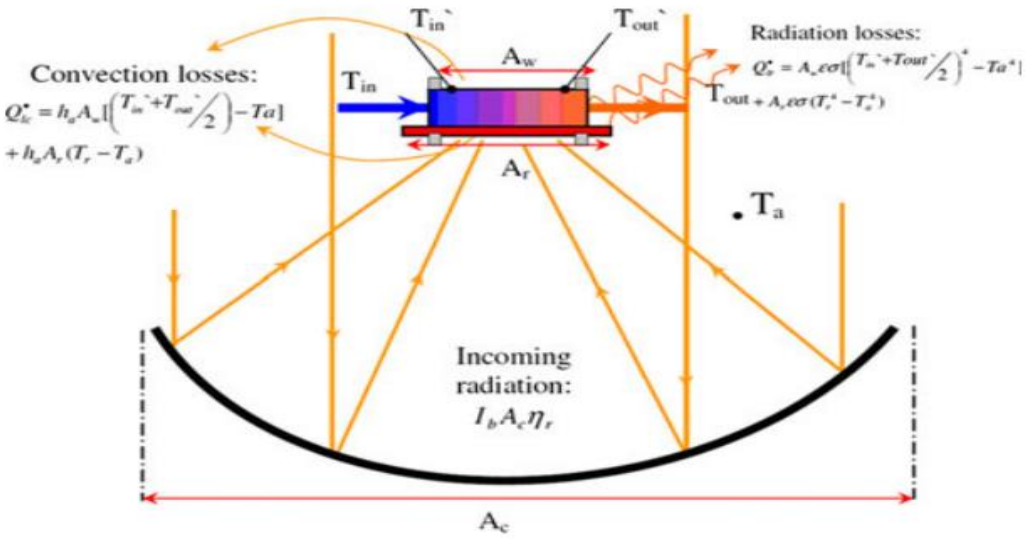

Figure 23: Schematic of the dish with the heat transfer system at the focal point.

II.3.3-Overall Efficiency of the CTEG system:

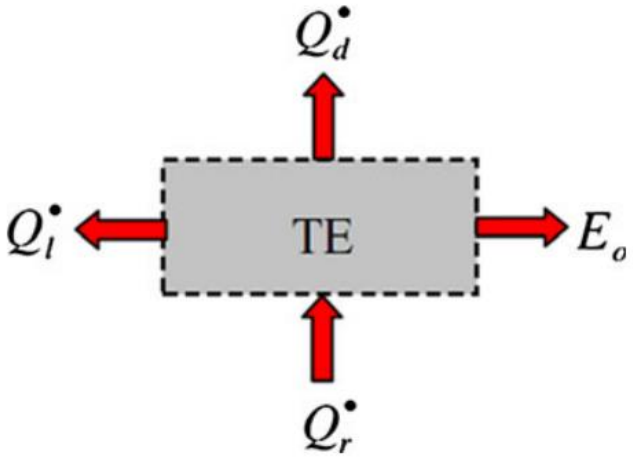

Figure 24: Energy balance for the thermoelectric generator.

Figure 3 illustrates the energy flow through the TEG module, which can be expressed by the energy balance as:

$$\dot{Q}_r = \dot{Q}_d + \dot{Q}_L + E_0 \tag{II.50}$$

Where $\dot{Q}_d$ is the unutilized heat dissipated from the cold side of the TEG module by the cooling system, which can be assumed to be equal to $\dot{Q}_w$ due to the low efficiency of the thermoelectric cells, and E_0 is the useful electric power produced by the TEG module.

Rearranging Eq. (14) gives:

$$\dot{Q}_r - \dot{Q}_L = \dot{Q}_d + E_0 \tag{II.51}$$

where the term $\dot{Q}_r$- $\dot{Q}_L$ on the left-hand side represents the actual heat flowing into the hot face of the TEG module. The electric power output by the thermoelectric generator can be expressed in terms of the generator efficiency as:

$$E = \eta_{teg}(\dot{Q}_r - \dot{Q}_L) \tag{II.52}$$

where $\eta_{teg} = \frac{E_0}{(\dot{Q}_r - \dot{Q}_L)}$ is the thermal to electrical efficiency of the TEG, as provided by the supplier as a function of the temperature difference between the hot and cold sides of the generator.

Figure 4 shows the details of the energy flow through the concentrator thermoelectric generator module. The waste heat dissipated from the cold side of the thermoelectric cells by the cooling system depends on the overall thermal resistance from the receiver plate where radiation is incident to the efficiency of the heat sink.

The total thermal resistance basically includes the conductive resistance through the receiver plate, the heat sink base, and the thermoelectric cells, and the convection resistance of the heat sink to the Air. Due to the high thermal conductivity of the Aluminum material used in the spreader and the heat sink, and the high heat transfer coefficient of the heat sink, the associated thermal resistances are very small.

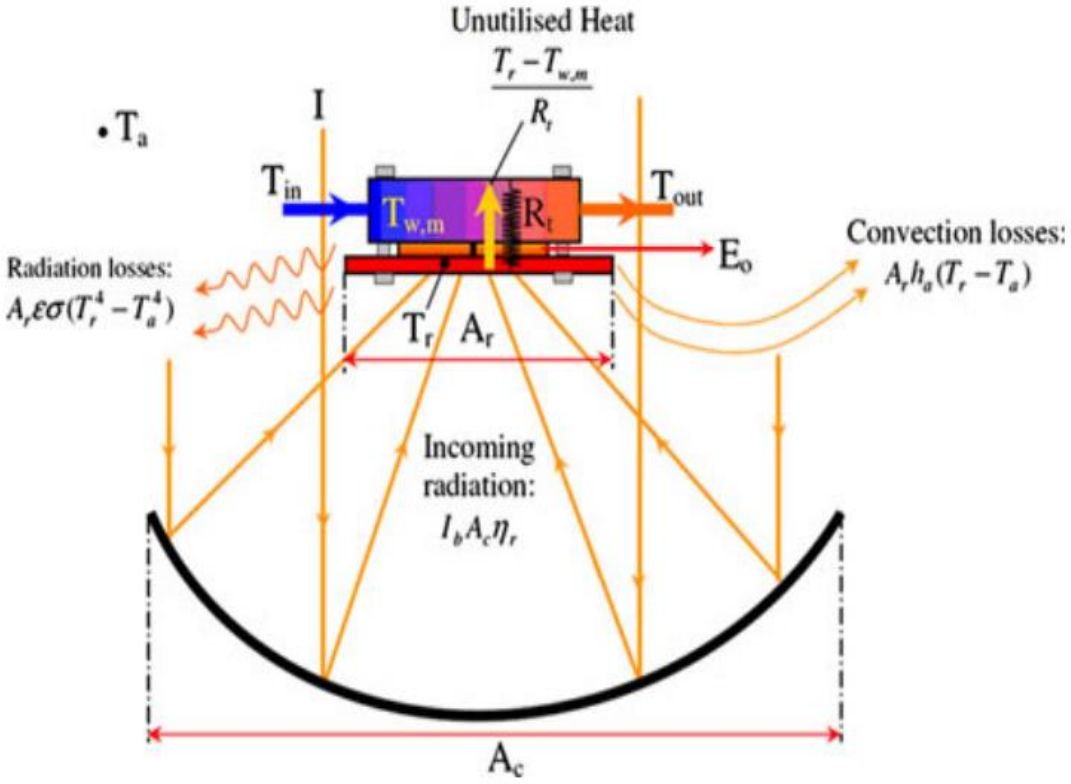

Figure 25: Energy flow in the concentrator thermoelectric generator module.

Chapter III: Experimental Setup

III.1-Hardware design:

III.1.1-The Solar Parabolic Dish Collector:

The higher cost of present solar dish concentrator system is limiting the users for utilization of solar thermal system.

The reductions in the system cost become possible by using outdated satellite dish antenna.

An unused satellite off-axis parabolic dish type (RCA 18" dish) has been used. The receiver plate was placed at the focus

The dish has a pole diameter of 32 mm, an offset angle of 24.62°, a 27.4 cm focus length, an aperture short axis of 46.1cm and aperture long axis of 50.7 cm.

The reflector surfaces were made painting and polishing the parabola with reflective chrome paint (60% reflective) on one side.

Figure 26: The solar parabolic thermoelectric generator

Figure 27: The solar parabolic dish reflective surface

III.1.2-Thermo Electric Generator (TEG)

The thermo electric generator is the heart of the electric module and is based on bismuth and telluride (BiTe) as n-type and p-type semiconductor.

BiTe cells are widely used as thermo electric units with low operating temperature range (< 160 C), high Seebeck coefficient (~ 190 µV/K) and high figure of merit (~ 2 x 10-3 K-1).

In the concentrator TEG system, one thermo electric cell with dimensions of 40 mm (L) x 40 mm (W) mm (T) and 127 p-n junctions were used.

Figure 28: BiTe thermo electric cell module

III.1.3-Tracking System:

To focus the solar rays' incident on the parabolic collector, the axis of the reflector should be parallel to the direction of incoming radiation at all times. In other words, the concentrator should track the sun continuously such that the solar influx is perpendicular to the collector aperture.

As mentioned above, the position of the sun in the sky at any time of the year can be located as the solar altitude (the angle between the sun's rays and the horizontal plane at the location) and the solar azimuth (the angle of the projection of the sun's rays onto the horizontal plane, measured clockwise from north).

These two angles are achieved by using a manual tracking mechanism arranged at the bottom of the dish.

The manual tracking mechanism works controlling each angle, both
being orchestrated manually synchronously.

Figure 29: Manual tracking of the sun

III.1.4-Heat transfer system :

The heat transfer system, as presented in Figs. 30 , 31 and 32, for the concentrator TEG module consists of two basic parts; (1) the receiver plate (Fig. 30), and (2) the heat sink (Fig. 31). The assembled heat transfer system is shown in Fig. 32.

A square Aluminum receiver plate (7.5 cm, 2mm thick) painted with black matt paint is positioned at certain distance below the focal point of the dish and helps to capture the radiation reflected from the collector and spread it evenly to the thermoelectric cell.

Due to the imperfect coating of the dish surface with reflective chrome paint, the reflected rays might not converge to a focal point.

As a result, the receiver plate dimension is larger than the surface area of the thermoelectric cell, to capture the maximum amount of reflected light.

The heat sink extracts the waste heat from the thermoelectric cells and thus helps to maintain the temperature of the cold face as low as possible.

Figure 30: Receiver plate

Figure 31: Heat sink

Figure 32: The assembled heat transfer system

III.2-Measurement instrumentations:

III.2.1-Temperature measurement:

Operating parameters such as receiver plate temperature, heat sink temperature, the space between them and ambient temperature are measured by using K type thermocouples made chromel-alumel measuring points as shown in Figure 33.

K type thermocouples are inexpensive, with a wide variety of probes and a range of (-200°C to +1350°C), having a sensitivity of approximately 41µV/°C and an accuracy of 0.1◦C.

Figure 33: Thermocouples on the measuring points

III.2.2-Data acquisition system:

Data from these instruments is to be acquired on timely basis by using Fluke data acquisition system. The accuracy of the system is shown in Figure.

Thermocouple		Accuracy (±°C)*				
		18°C to 28°C			0°C to 60°C	
Type (°C)	Temperature (°C)	90 Days Slow	1 Year Slow	1 Year Fast	1 Year Slow	1 Year Fast
J	-100 to -30	0.44	0.45	0.92	0.57	1.10
	-30 to 150	0.41	0.43	0.83	0.61	1.06
	150 to 760	0.48	0.53	0.98	0.92	1.42
K	-100 to -25	0.53	0.54	1.14	0.66	1.33
	-25 to 120	0.46	0.48	0.96	0.66	1.19
	120 to 1000	0.79	0.85	1.55	1.45	2.20
	1000 to 1372	1.32	1.42	2.30	2.29	3.23
N	-100 to -25	0.63	0.64	1.44	0.75	1.61
	-25 to 120	0.53	0.54	1.21	0.66	1.39
	120 to 410	0.45	0.48	1.05	0.73	1.30
	410 to 1300	0.88	0.95	1.70	1.63	2.41

Figure 34: Fluke data acquisition system accuracy

Figure 35: Fluke data acquisition system

III.2.3-Solar Radiation and wind velocity measurement:

Solar beam radiation is measured by a pyranometer as mentioned before with an accuracy of 0.1%.

The wind velocity is measured by the wind anemometer (Model: FESTO 45).

III.2.4-Electrical measurement:

The generated voltages, electrical current and connected electrical load of TEG are measured by using the digital multimeter (Fluke).

Accuracy and specifications of the multimeter are shown in the figure.

Accuracy specifications	
DC voltage	**Range** 0.1 mV to 1000 V **Accuracy** 0.25 % + 2
AC voltage	**Range** 0.1 mV to 1000 V **Accuracy** 1.0 % + 3
DC current	**Range** 1 mA to 10 A **Accuracy** 1.0 % + 3
AC current	**Range** 1 mA to 10 A **Accuracy** 1.5 % + 3
Resistance	**Range** 0.1 Ω to 40 MΩ
Counts	6000
Capacitance	**Range:** 1 nF to 9999 µF **Resolution:** 1nF
Frequency	**Range:** 5 Hz to 50 kHz **Resolution:** 0.01Hz
Temperature	-40 °C to +400 °C
Power	AA batteries: Three for main body; two for display
Battery life	400 hours
Wireless frequency	2.4 GHz ISM Band 10 meter range
Safety rating	CAT IV 600 V , CAT III 1000 V

Figure 36: Fluke multimeter specifications

Figure 37: The used Fluke multimeter

III.3-Testing Procedure:

Figure 38: The STEG during the test

- In order to determine the source resistance of the thermoelectric module to load match, the system's AC resistance was measured in an open circuit and determined to be 3.45 Ω. The thermal conductivity was found to be 1.37 W/m/K when averaging directional thermal conductivities [34], leading to a thermal conductance of 4.89 W/K using the dimensional properties of the module. Using the open circuit voltage versus hot side temperature curve for the module (shown in Figure 35) and determining the slope over the STEG's operating temperature range, the total Seebeck coefficient of the module was determined to be 46.6 mV/K.

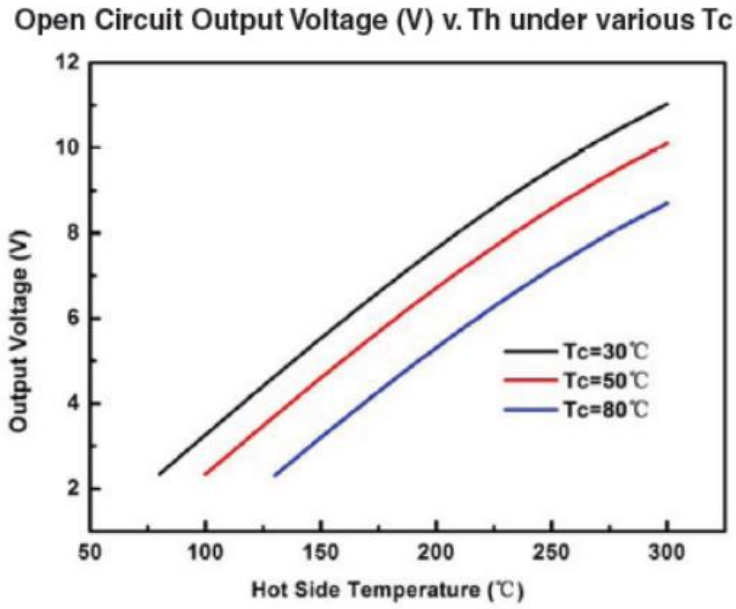

Figure 39: Performance Curve for Thermoelectric Module [35]

- **Open Circuit Test:**

  - The first test of the STEG was an open circuit outside under the ambient conditions, connecting the module output wires to the acquisition system. The open circuit voltage and current were recorded for given time intervals along with the temperature of the receiver, the heat sink and the space between them.
    The maximum output power recorded during the open circuit test was 2.153W.
  - Another open circuit test was done only this time it was indoor heating the receiver with a heating plate applying a 100W power for first experimentation and a 750W on the second one.

- **Loaded Circuit Test:**

  - Sarah watzman conducted 2 outdoor loaded circuit tests using 4 thermoelectric elements in a STEG [16].
    For the first test outdoor; the STEG reached a steady-state open circuit voltage of 0.660 V in approximately 60 minutes. The input solar flux was measured at 834 W/m², the maximum output power was 0.0209 W, and the peak system efficiency was 0.0293%.
    For the second loaded test, the input solar flux was measured at 750 W/m², the maximum power output was 0.0191 W, and the peak system efficiency was 0.0299%. These results are summarized in Figure 40.

	Loaded Test 1	Loaded Test 2
Input Solar Flux (W/m^2)	834	750
Input Solar Power (W)	71.16	63.99
Open Circuit Voltage (V)	0.660	0.640
Maximum Power Output (W)	0.0209	0.0191
Heat Losses (W)	71.14	63.97
Peak Module Efficiency	0.0302%	0.0285%
Peak System Efficiency	0.0293%	0.0299%

Figure 40: Sarah Watzman's Loaded Outdoor Tests Results [16]

  - Based on the results of previous experimentation works such as Watzman's [16], Hongnan Fan et al [9] and M.Eswaramoorthy et al [17]. We've estimated the loaded circuit current and voltage peaks to be 90% of the open circuit peaks.

III.3.1-Results and analysis:

- **The system's thermal efficiency:**

The different measures we had allowed us to evaluate the system's thermal actual efficiency and how does it affect our STEG's global efficiency.

The next figures will present the temperatures measured vs. the different parameters that influenced it (such as beam radiation and wind velocity).

- The parabolic dish efficiency was not as expected since we got a maximum temperature of 168°C on the receiver at the maximum beam radiation (911, 6078 W/m²) as shown in Figure 41, and that is due to the reflective surface (commercial chrome paint) reflectivity which has been remarkably bad, and receiver's absorbance and emissivity which was not quite good due to the black paint used to paint. However the thermal conductivity of the Aluminum was good enough to transfer the heat from and to the TEG.
- The heat sink efficiency was acceptable taking in consideration that it's a passive cooling system.

  The system responded positively to the wind velocity as shown in Figure 42 giving a temperature difference up to 90°C.

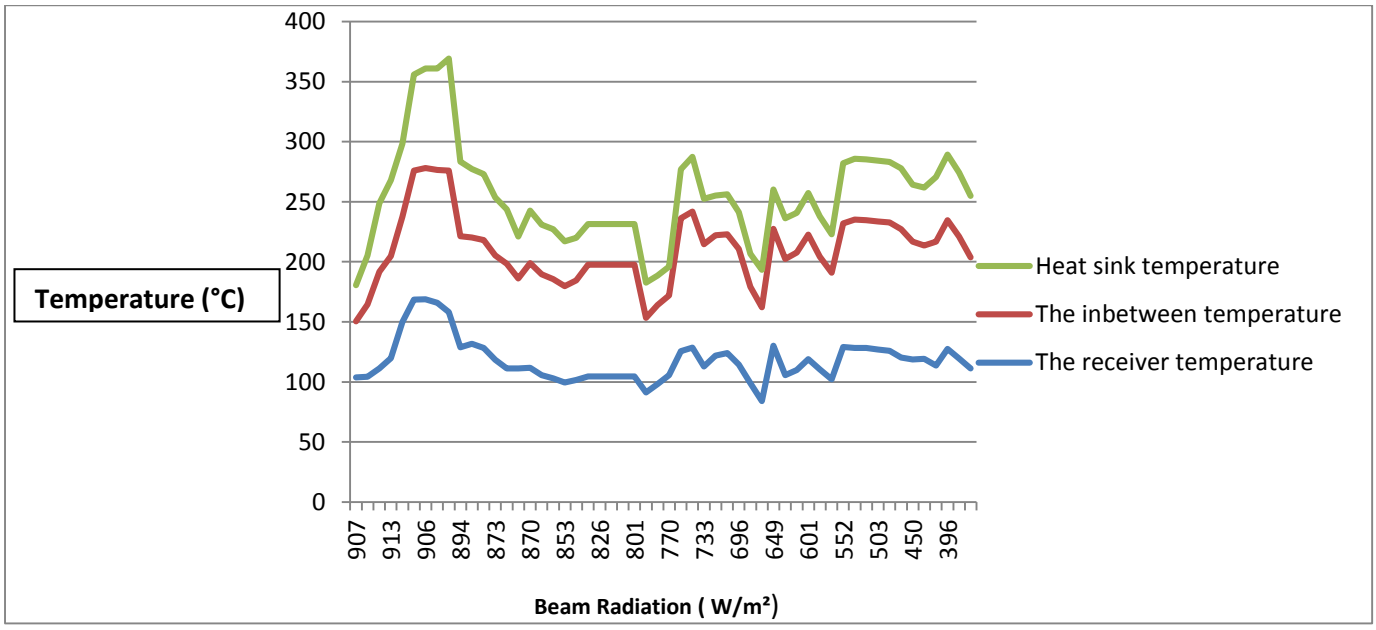

Figure 41: The different heat system measured temperatures (°C) vs. the beam radiation (W/m²)

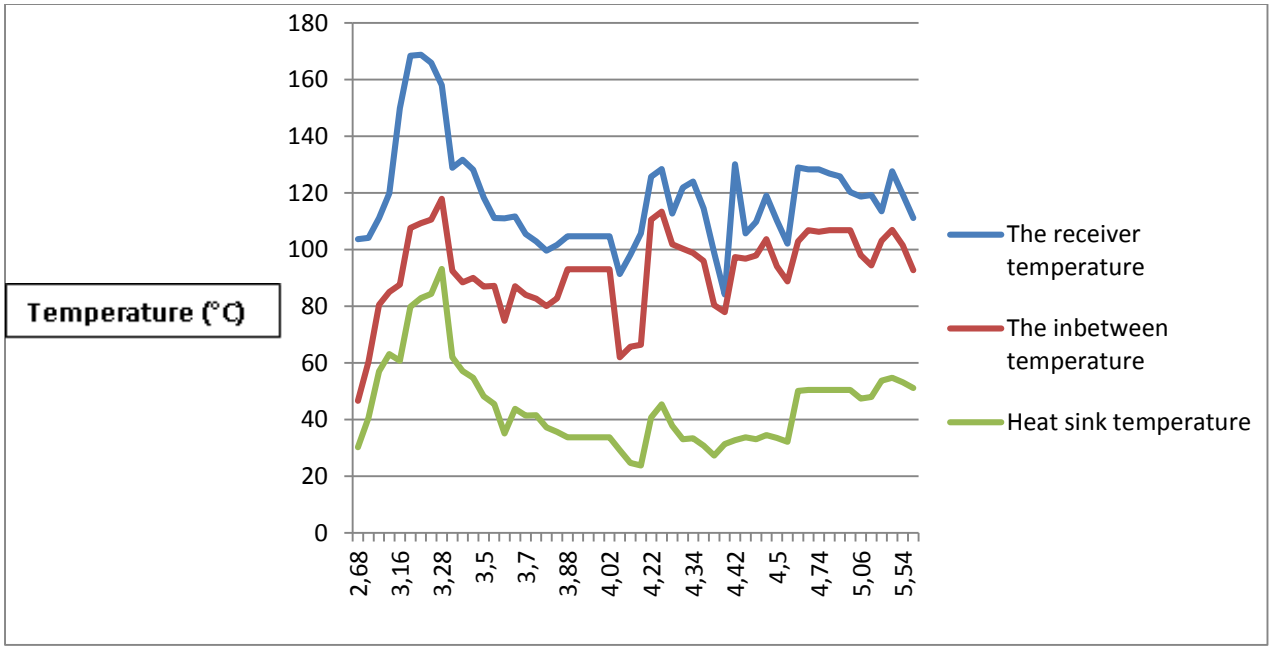

Figure 42: The different heat system measured temperatures (°C) vs. the wind velocity (m/s)

- **Open Circuit Test:**
  - An open circuit indoor test done by Sarah Watzman [16] using 4 thermoelectric elements showed that the system tested reached the steady state in about 80min giving a voltage peak of 4.54mV as shown in Figure 43.

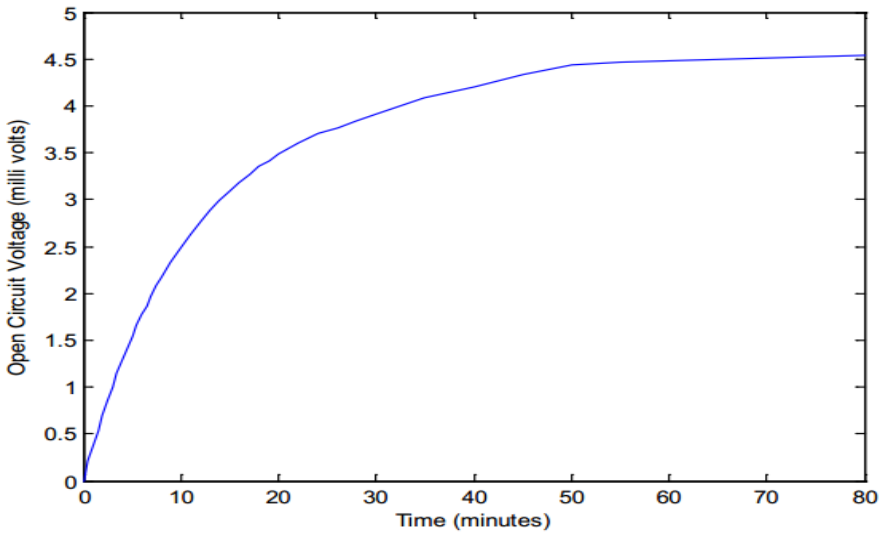

Figure 43: The Sarah Watzman's Circuit Voltage Results for Indoor Test [16]

- In our open circuit test we reached 0.77V voltage peak for the 100W test giving a 0.192W power generation and 0.19% efficiency.
  And a 1.7 voltage peak for the 750W test giving a 0.85W power generation and 0.11% efficiency.
- However in our outdoor open circuit test we reached some interesting results.
  A voltage peak up to 2.75V and a power generation of 2.075W and an efficiency of 0.41% in a beam radiation of 900 W/m² and temperature difference of 78°C as shown in Figure 44 and Figure 45.
- In the results we can clearly see the influence of the beam radiation on the output power which gives eligibility to the STEG.

PS: the instability in the results and the massive sudden changes is due the manual tracking system errors.

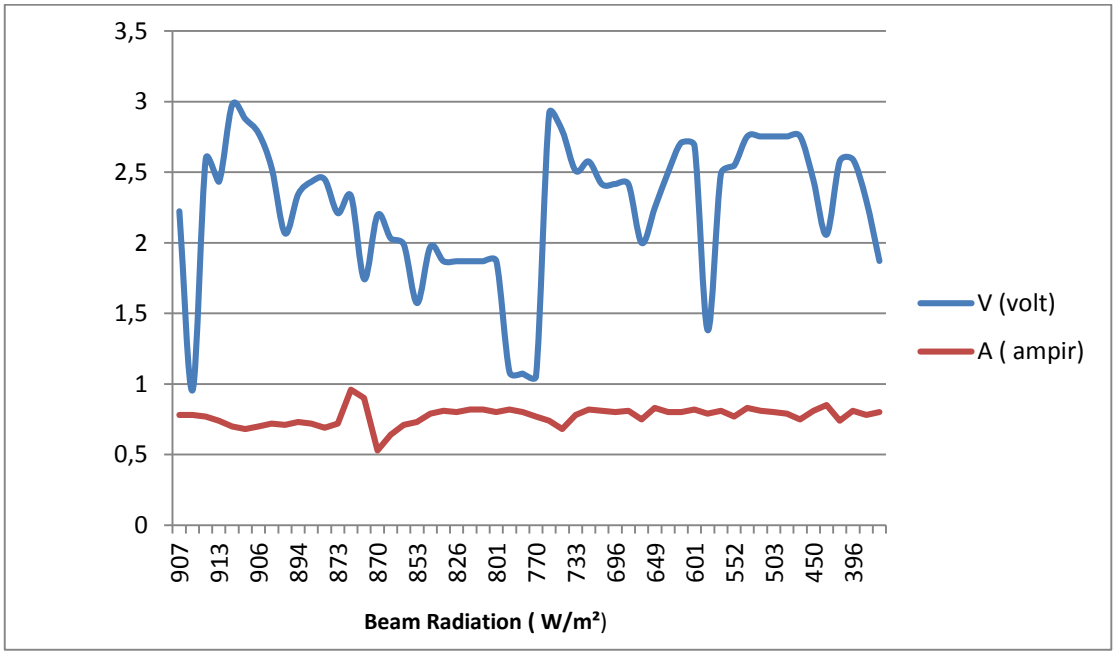

Figure 44: Open circuit voltage (volt) and current (Ampere) vs. Beam radiation (W/m²)

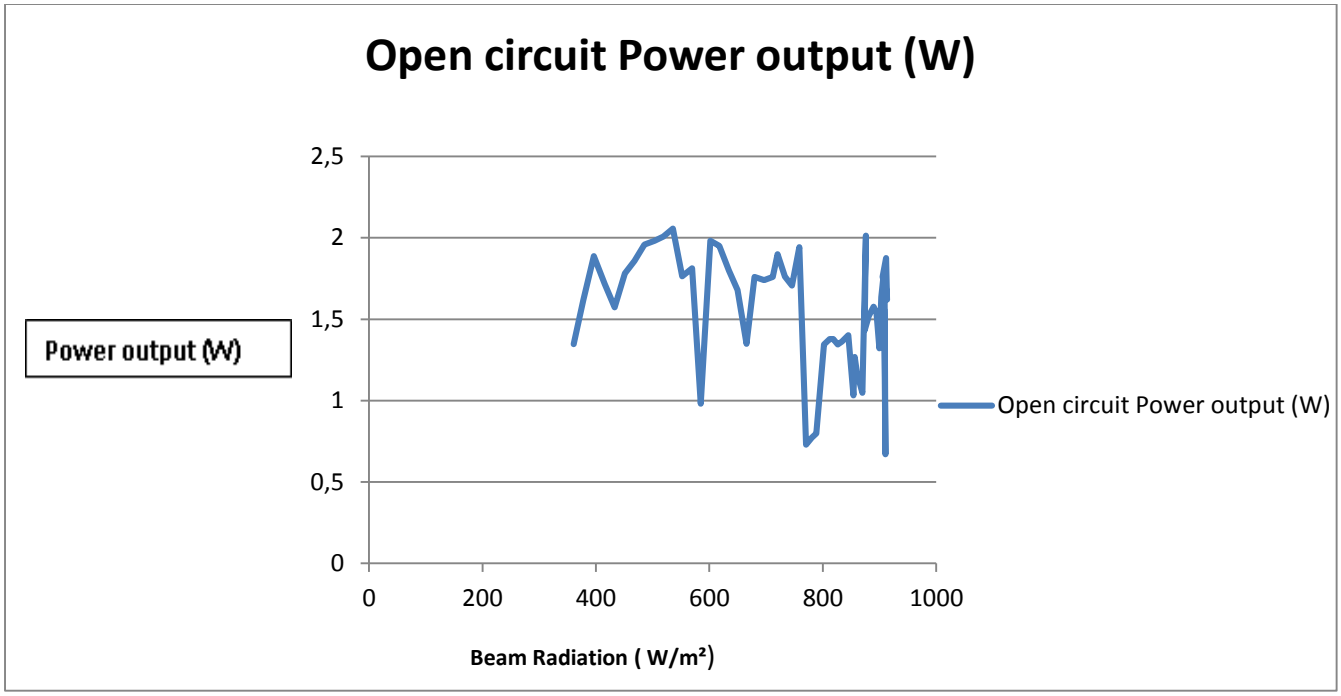

Figure 45: Open circuit power output (w) vs. Beam radiation (W/m²)

- **Loaded circuit test :**
  - As mentioned before based on previous works we've estimated the loaded circuit voltage and current peaks to be 90% of the closed circuit peaks.
  - In our outdoor loaded circuit test we reached some interesting results. A voltage peak up to 2.475V and a power generation of 1.8675W and an efficiency of 0.37% in a beam radiation of 900 W/m² and temperature difference of 78°C as shown in Figure 46 and Figure 47.
  - In the results we can clearly see the influence of the beam radiation on the output power which gives eligibility to the STEG.

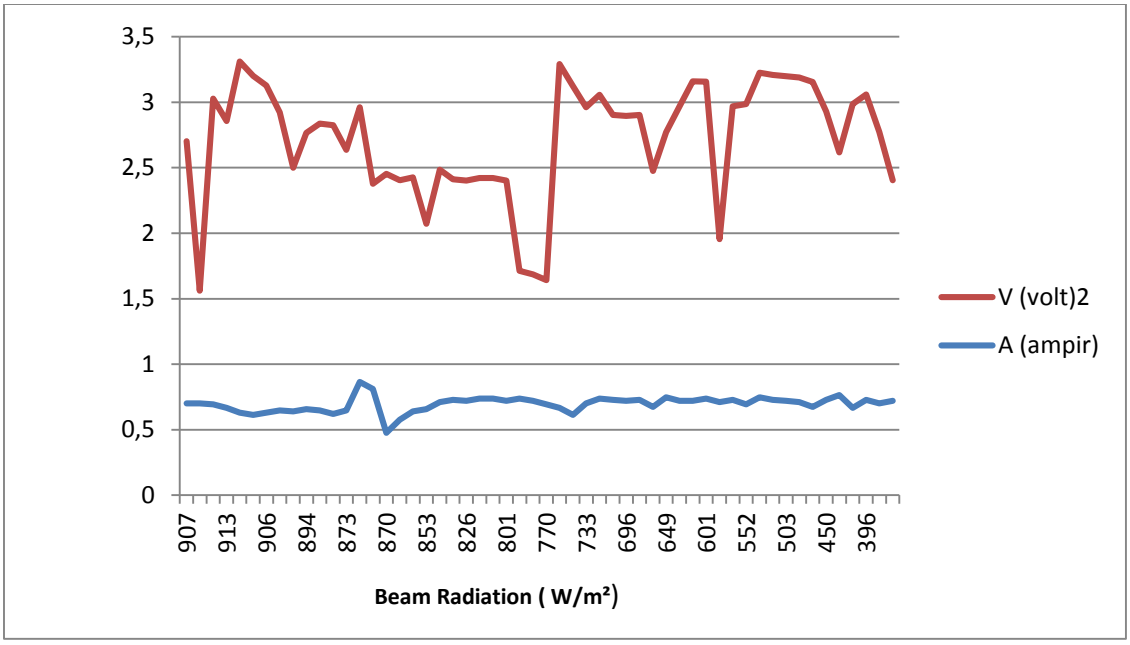

Figure 46: Loaded circuit voltage (Volt) and current (Ampere) vs. Beam radiation (W/m²)

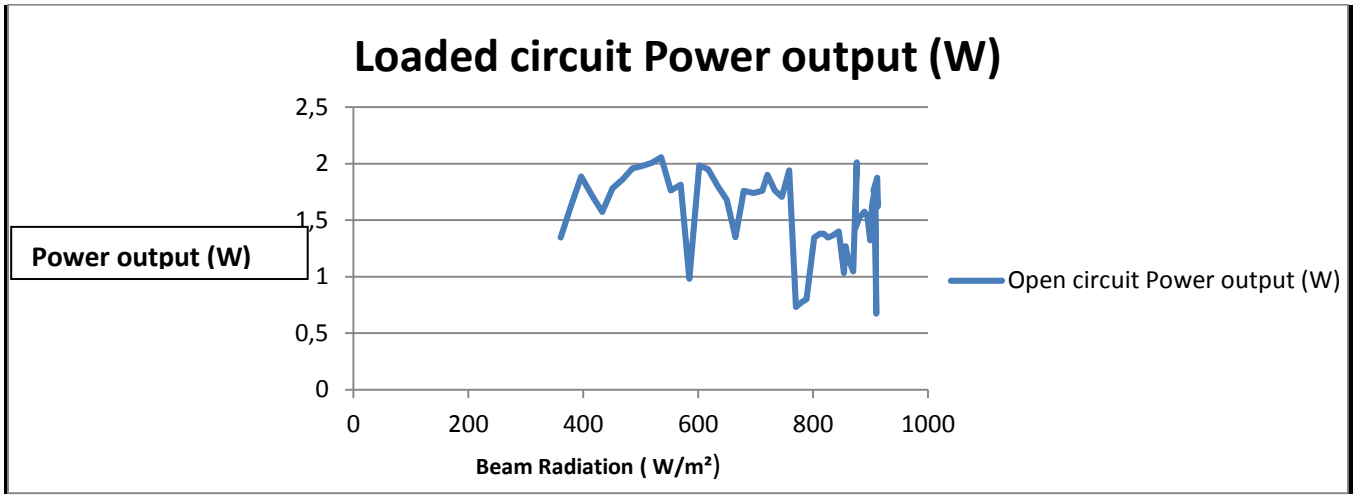

Figure 47: Loaded circuit power output (w) vs. Beam radiation (W/m²)

- Although the obtained results and efficiency are a bit small, but they are considered above the average compared to some other similar experimentations.

PS: the instability in the results and the massive sudden changes is due the manual tracking system errors.

Conclusions and Recommendations:

- Our parabolic dish concentrator optical efficiency was not up to the expectations due to the poor reflective surface (commercial chrome paint) which has a direct affection on our system's heat efficiency.
  We recommend the use of better reflective and more effective reflective surfaces in the future works.
- Also the concentrator tracking system presented a challenge in which we had to overcome by using a manual tracking system. a system that costs financially less but not so effective and causes so much perturbations as it can be seen in the tests results.
  We recommend considering a better tracking system in future works.
- As it was demonstrated in the tests, the thermoelectric module allowed too much heat to flow through it to maintain the steady-state temperature gradient, consequently increasing the temperature of the heat sink and decreasing the temperature gradient. This ultimately cause the voltage produced by the module to decrease.
  In order to avoid this problem and increase the STEG efficiency, the heat sink needs big capability to dissipate heat, which could be achieved through a finned heat sink or a heat sink with water cooling.
  Our system's heat sink was effective taking in consideration that it was a passive system working on the natural air convection only , with a low cost and a better efficiency when wind velocity is to increase as demonstrated in the tests.
- In order to reach the STEG's maximum power output, the load resistance should equal the source resistance (as it was proven by analyzing pervious works [16]). Yet this is not the case for maximum thermal efficiency.
- The efficiency of the STEG in previous works has reached some very important levels (12% [9]) comparing to the efficiency that our system reached (0.37%).
  However, it is still considered a positive result comparing to some other works and to the hardware used.
- For STEGs to enter the consumer solar energy market and be competitive with photovoltaics, which currently dominate this market [2], STEG efficiency needs to greatly increase and at least match current efficiencies found in photovoltaic solar panels.
  For common crystalline silicon solar cells, efficiency is standardly 12% [18].
  Considering that MIT's peak efficiency was measured at 5.2% [2] and only 0.03% for this research, room for major improvements exists before STEGs can even begin to compete.

References :

[1]: cours de thermoélectricité,Université de Pau et des Pays de l'Adour France

[2]: MacDonald, D. K. C. Thermoelectricity: An introduction to the principles. 1962. New York: John Wiley & Sons, Inc.

[3] A. Volta, "Nuova memoriaSull' elettricitaaanimale. Divisa in treletterediretta al signor Abate Anton Maria Vassali, proffessore di fisicanella R. Université Torino. 1794-1795." Institute for experimental medicine of Russia — «A.Galvani and A.Volta, selected papers on animal electricity», OGIZ Publ., M.— L., 1937., 1795-1794.

[4] T. J. Seebeck, "MagnetischePolarisation der Metalle und ErzeDurchTemperaturDifferenz," in Ostwald's Klassiker der ExaktenWissenshaftenNr. 70 (1895). Seebeck
Biography 1. Seebeck Biography2., 1822.

[5] J. C. Peltier, "Nouvelles expériences sur la caloricité des courants électriques," p. I. VI (1834) 371–87.

[6] E. Altenkirch, "Electrotehrmischekalteerzeugung und reversible elektrischeHeizung," p. 12 (1911) 920–4.

[7]:(Rowe, 1995)

[8]:(Riffat& Ma, 2003).

[9]:Hongnan Fan, Randeep Singh, AliakbarAkbarzadeh . Power Generation from Thermoelectric Cells by Using HighConcentrated Solar Dish. Proceedings of the Solar10, the 48th ANZSES Annual Conference,1 Dec – 3 Dec, 2010

[10]:Thermoelectrics. 2013. California Institute of Technology: Materials Science. <http://thermoelectrics.caltech.edu/thermoelectrics/engineering.html>.

[11]: Telkes, M. The Efficiency of Thermoelectric Generators. Journal of Applied Physics 18, 1116-27. 1947.

[12]: J. Chen, J. Appl. Phys. 79, 5 (1996).

[13]: Telkes, M. Solar Thermoelectric Generators. Journal of Applied Physics 25, 765-77. 1954.

[14]:Goldsmid, H. J. Thermoelectric Applications of Semiconductors. Journal of Electronics and Control 1(2), 218-22. 1955.

[15]: Goldsmid, H. J., et al. Solar Thermoelectric Generation Using Bismuth Telluride Alloys. Solar Energy 24, 435-440. 1979.

[16]: Sarah Watzman ,Design of a Solar Thermoelectric Generator, April 4th, 2013

[17]: M.Eswaramoorthy1, S.Shanmugam2, AR.Veerappan3 ,Experimental Study on Solar Parabolic DishThermoelectric Generator , Jun. 2013, Vol. 3 Iss. 3, PP. 62-66

[19]: A.Vienne,- Introduction à l'Astronomie. LAL-IMCCE Laboratoire d'Astronomie de Lille de l'Institut de
Mécanique Céleste et de Calcul des Ephémérides, Lille 1 et Observatoire de Paris, UMR 8028 du CNRS. (6)

[20]: A.Bertrand,- Exploitation Des Nouvelles Capacités D'observation De La Terre Pour Evaluer Le Rayonnment Solaire Incident Au Sol, Thèse de Doctorat, ED N° 432 : "Science des Métiers de l'Ingénieur", école nationale supérieure des mines de Paris.(7)

[21]: M. Capderou, 'Atlas Solaire de l'Algérie', Modèles Théoriques et Expérimentaux, Vol. 1, T1, Office des Publications Universitaires, EPAU, Algérie, 375 p., 1987. (4)

[22]: F. Yettou, A. Malek, M. Haddadi, A. Gama – Etude comparative de deux modèles de calcul du
rayonnement solaire par ciel clair en Algérie, Revue des Energies Renouvelables Vol. 12 N°2 (2009) 331 – 346.(20)

[23]: K. Daniel, L. Gautret,- Génération du Disque Solaire des Communes de l'Ouest, ARER, Mars- Août 2008.(5)

[24]: O. Aissani, A. Mokhnache - Application de la télédétection pour étudier l'effet des aérosols
atmosphériques sur le rayonnement solaire global, Revue des Energies Renouvelables Vol. 11 N°1 (2008) 65 – 73. (32)

[25]: Bernard, R., Menguy, G and Schwartz, M.-1980- Le Rayonnement Solaire : Conversion Thermique et Application. Technique et Documentation, Paris. 215 p (1)

[26]: Ch.Perrin de Brichambrant et Ch.Vauge, ''Le gisement solaire. Evaluation de la ressource énergétique'', Technique et Documentation Lavoisier Paris 1982.(36)

[27]: M.R. Yaïche, S.M.A. Bekkouche - Conception et validation d'un programme sous Excel pour l'estimation du rayonnement solaire incident en Algérie. Cas d'un ciel totalement clair, Revue des Energies Renouvelables Vol. 11 N°3 (2008) 423 – 436.(19)

[28]: L.Diabaté, J. Remund, L. Wald - Linke Turbidity Factors For Several Sites In Africa, Diabaté L., Remund J., Wald L., 2003. Linke Turbidity Factors For Several Sites In Africa. Solar Energy, 75, 2, 111- 119.

[29]: M.R Yaïche, S.M.A Bekkouche - Estimation du rayonnement solaire global en Algérie pour différents types de ciel, Revue des Energies Renouvelables Vol. 13 N°4 (2010) 683 – 695. (23)

[30]: La Météorologie 8e 42 série - n° 31 - septembre 2000 de Pierre Bessemoulin et Jean Oliviéril.

[31]:SerkanKapucu,Concentrating Collectors, PHYS 471Solar Energy □2004-1

[32]: Chapter 7 of Solar Engineering of thermal processes by Duffie& Beckman, Wiley, 1991

Reference

[33]: Paul Wade N1BWT, OFFSET-FED PARABOLIC DISH ANTENNAS, 1995-1998

[34]: Scherrer, H. and S. Scherrer. CRC Handbook of Thermoelectrics. Ed. D. M. Rowe. 1995. Boca Raton, FL: CRC Press.

[35]: G2-35-0315 Thermoelectric Module Specifications. Traverse City, MI: Tellurex.